

Alma Mater Studiorum Università di Bologna
Archivio istituzionale della ricerca

Addressing a Trapped High-Energy Water: Design and Synthesis of Highly Potent Pyrimidoindole-Based Glycogen Synthase Kinase-3 β Inhibitors

This is the final peer-reviewed author's accepted manuscript (postprint) of the following publication:

Published Version:

Addressing a Trapped High-Energy Water: Design and Synthesis of Highly Potent Pyrimidoindole-Based Glycogen Synthase Kinase-3 β Inhibitors / Andreev S.; Pantsar T.; Tesch R.; Kahlke N.; El-Gokha A.; Ansideri F.; Gratz L.; Romasco J.; Sita G.; Geibel C.; Lammerhofer M.; Tarozzi A.; Knapp S.; Laufer S.A.; Koch P.. - In: JOURNAL OF MEDICINAL CHEMISTRY. - ISSN 0022-2623. - ELETTRONICO. - 65:2(2022), pp. 1283-1301. [10.1021/acs.jmedchem.0c02146]

Availability:

This version is available at: <https://hdl.handle.net/11585/838473> since: 2024-03-11

Published:

DOI: <http://doi.org/10.1021/acs.jmedchem.0c02146>

Terms of use:

Some rights reserved. The terms and conditions for the reuse of this version of the manuscript are specified in the publishing policy. For all terms of use and more information see the publisher's website.

This item was downloaded from IRIS Università di Bologna (<https://cris.unibo.it/>).
When citing, please refer to the published version.

(Article begins on next page)

This is the final peer-reviewed accepted manuscript of:

Andreev S, Pantsar T, Tesch R, Kahlke N, El-Gokha A, Ansideri F, Grätz L, Romasco J, Sita G, Geibel C, Lämmerhofer M, Tarozzi A, Knapp S, Laufer SA, Koch P.

Addressing a Trapped High-Energy Water: Design and Synthesis of Highly Potent Pyrimidoindole-Based Glycogen Synthase Kinase-3 β Inhibitors.

J Med Chem. 2022 Jan 27;65(2):1283-1301.

The final published version is available online at:
<https://doi.org/10.1021/acs.jmedchem.0c02146>

Terms of use:

Some rights reserved. The terms and conditions for the reuse of this version of the manuscript are specified in the publishing policy. For all terms of use and more information see the publisher's website.

This item was downloaded from IRIS Università di Bologna (<https://cris.unibo.it/>)

When citing, please refer to the published version.

Addressing a Trapped High-Energy Water: Design and Synthesis of Highly Potent Pyrimidoindole-based GSK-3 β inhibitors

Stanislav Andreev^{1,‡}, **Tatu Patsar**^{1,2,‡}, **Roberta Tesch**^{3,4}, **Niclas Kahlke**¹, **Ahmed El-Gokha**^{1,5}, **Francesco Ansideri**¹, **Lukas Grätz**⁶, **Jenny Romasco**⁷, **Giulia Sita**⁸, **Christian Geibel**⁹, **Michael Lämmerhofer**⁹, **Andrea Tarozzi**⁷, **Stefan Knapp**^{3,4}, **Stefan A. Laufer**^{1,10} and **Pierre Koch**^{1,6,*}

¹ Institute of Pharmaceutical Sciences, Department of Medicinal and Pharmaceutical Chemistry, Eberhard Karls University Tübingen, Auf der Morgenstelle 8, 72076 Tübingen, Germany

² School of Pharmacy, Faculty of Health Sciences, University of Eastern Finland, P.O. Box 1627, 70211 Kuopio, Finland

³ Institute for Pharmaceutical Chemistry, Johann Wolfgang Goethe-University, Max-von-Laue-Str. 9, 60438 Frankfurt am Main, Germany

⁴ Structural Genomics Consortium, Buchmann Institute for Life Sciences, Johann Wolfgang Goethe-University, Max-von-Laue-Str. 15, 60438 Frankfurt am Main, Germany

⁵ Chemistry Department, Faculty of Science, Menoufia University, Gamal Abdel-Nasser Street, 32511 Shebin El-Kom, Egypt

⁶ Department of Pharmaceutical/Medicinal Chemistry II, Institute of Pharmacy, University of Regensburg, Universitätsstraße 31, 93053 Regensburg, Germany

⁷ Department for Life Quality Studies, Alma Mater Studiorum, University of Bologna, Corso D'Augusto 237, 47921 Rimini, Italy

⁸ Department of Pharmacy and Biotechnology, Alma Mater Studiorum, University of Bologna, Via Irnerio 48, 40126 Bologna, Italy

⁹ Institute of Pharmaceutical Sciences, Department of Pharmaceutical (Bio-)Analysis, Eberhard Karls University Tübingen, Auf der Morgenstelle 8, 72076 Tübingen, Germany

¹⁰ Tübingen Center for Academic Drug Discovery (TüCAD2), Auf der Morgenstelle 8, 72076 Tübingen, Germany

‡ These authors contributed equally.

Abstract

In small molecule binding, water is not a passive bystander but rather takes an active role in the binding site that may be decisive for inhibitor potency. Here, by addressing a high-energy water, we improved the IC₅₀ value of our co-crystallized glycogen synthase kinase-3 β (GSK-3 β) inhibitor by nearly two-orders of magnitude. Surprisingly, our results demonstrate that this high-energy water was not displaced by our potent inhibitor (*S*)-3-(3-((7-ethynyl-9*H*-pyrimido[4,5-*b*]indol-4-yl)(methyl)amino)piperidin-1-yl)propanenitrile (**(*S*)-15**, IC₅₀ value of 6 nM). Instead, only a subtle shift in the location of this water molecule resulted in a dramatic decrease in energy of this high-energy hydration site based on the WaterMap analysis combined with microsecond timescale molecular dynamics simulations. **(*S*)-15** demonstrated a favorable kinome selectivity profile, target engagement in a cellular environment, and reduced GSK-3 autophosphorylation in neuronal SH-SY5Y cells. Overall, these findings highlight that even a slight adjustment in a high-energy water location can be decisive for ligand binding.

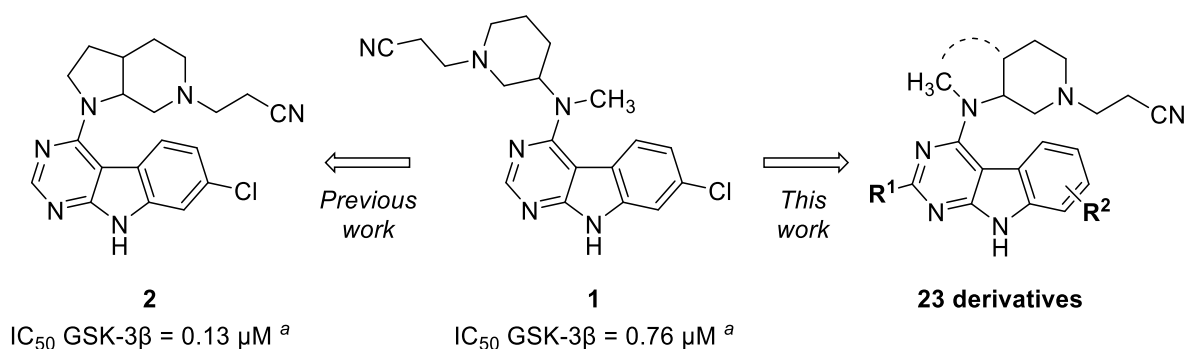
Keywords: Glycogen Synthase Kinase 3 beta; 9*H*-pyrimido[4,5-*b*]indole, WaterMap, Molecular Dynamics Simulation

Introduction

Protein kinases are important regulators in the cellular signaling machinery.¹ Aberrations in their activity can lead to disease, and they are considered as potential drug targets in many therapeutical areas, including cancer, degenerative disorders as well as autoimmune and inflammatory diseases.² Therefore, perhaps unsurprisingly, protein kinases are currently the most pursued drug targets in the pharmaceutical industry.³

During the last decades, in particular glycogen synthase kinase-3 β (GSK-3 β) has received extensive attention both from academia and industry.⁴⁻⁷ This serine/threonine kinase is a highly multitasking enzyme that contributes to several key signaling pathways in cells.⁸ GSK-3 β dysregulation has been associated with various pathologies such as type II diabetes mellitus, various types of cancer and Alzheimer's disease.⁹⁻¹¹ Therefore, determined efforts are ongoing to develop selective inhibitors against GSK-3 β .

We recently reported optimization of a novel class of 7-chloro-9*H*-pyrimido[4,5-*b*]indole-based inhibitors of GSK-3 β .¹² In this study, we revealed the cyanoethyl substituted piperidine (**1**) as an essential motif for the compound activity, which was further improved by a rigidification approach (**2**). Having identified the optimal structural features for the aliphatic side chain of the molecules, we herein pursued to optimize decorations at the 9*H*-pyrimido[4,5-*b*]indole core.



Scheme 1. Previously reported optimization of the aliphatic side chain. ^a Data taken from Andreev *et al.*¹²

Water is a vital component in the biological matrix that plays various important roles in molecular biology.¹³ This is especially true at the protein interface, as water plays a pivotal role in ligand binding thermodynamics.¹⁴⁻¹⁹ As solvent organization may be decisive for the binding affinity,²⁰⁻²¹ exploiting water offers an excellent opportunity to optimize ligand binding. However, not all waters are equal at the protein interface. While a displacement of an energetically favorable water molecule from the binding site by the ligand has a negative impact on binding affinity, it is highly beneficial in the case of energetically unfavorable water molecules. Therefore, it is essential to estimate the energies of these molecules before aiming for their displacement. There are a rising number of computational methods that aim to predict hydration site energies and thereby guide the decision for a beneficial water molecule displacement.²²⁻²³ One such method is WaterMap,²⁴⁻²⁵ which evaluates the hydration site energies based on a short molecular dynamics (MD) simulation where non-solvent heavy atoms are restrained. This method has been successfully applied in several instances related to protein kinases, such as with Platelet Derived Growth Factor Receptor- β (PDGF-R β),²⁶ p38 α MAP kinase,²⁷ Dual-specificity tyrosine phosphorylation-regulated kinase (DYRK),²⁸ kinase inhibitor selectivity among four kinases,²⁹ inhibitor selectivity among phosphoinositide 3-kinases (PI3Ks),³⁰ Cyclin G-Associated Kinase (GAK),³¹ Janus kinases (JAKs),³² and Interleukin-1 Receptor Associated Kinase 4 (IRAK4).³³

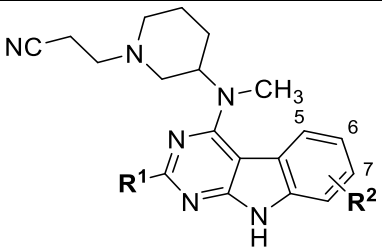
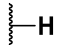
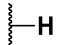
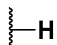
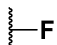
Here we applied a water-guided ligand-design approach in the development of highly potent inhibitors of GSK-3 β . By exploiting a new co-crystal structure (PDB 7B6F) in combination with WaterMap and MD simulations, we were able to improve the potency of our 9*H*-pyrimido[4,5-*b*]indole based compounds by almost two orders of magnitude, resulting in single-digit nanomolar IC₅₀ values. Remarkably, our results demonstrate how a small shift in the location of a high-energy water molecule by the ligand was highly beneficial. This strategy of inducing a subtle shift for an isolated high-energy water molecule in a lipophilic environment

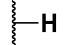
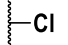

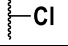

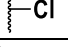



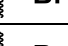

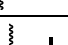
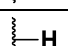
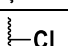
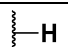

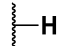
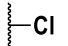
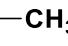
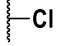
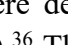
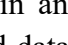
introduces a new tool for water-targeted ligand design, in addition to the canonical solvent displacement, replacement or interaction.³⁴

Results

Our initial structural modifications on the tricyclic scaffold of **1** were mainly focused on the third non-heteroaromatic ring of the 9*H*-pyrimido[4,5-*b*]indole tricycle (Table 1). The exchange of the chlorine atom in the 7-position with fluorine or bromine as well as its complete removal were well tolerated and generally provided triple-digit nanomolar GSK-3 β inhibitors (**5a-d**). Only the corresponding 7-iodine derivative (**11**) displayed diminished activity. In contrast, the relocation of the chlorine or bromine substituent to the 6-position (**5g** and **5h**) or 5-position (**5i**) was associated with a substantial (5–10 fold) decrease in potency. Furthermore, the introduction of a methyl group in the pyrimidine 2-position of parent compound **1** afforded an inactive derivative (**5j**, IC₅₀ value > 10 μ M). As we recently observed a strong influence of the stereoconfiguration on the bioactivity of structurally related GSK-3 β inhibitors,³⁵ we also decided to evaluate the activity of enantiopure compounds within this series. Here, however, this effect was not that strong. Nevertheless, respective *S*-enantiomers of **1** (= **rac-5c**) and **5d** displayed a slight trend for improved IC₅₀ values (1.5 and 1.3-fold, respectively).

Table 1. Structures and biological activities of halogen substituted compounds.

							
No.	R ¹		R ²	GSK-3 β IC ₅₀ \pm SEM [μ M] ^a	pIC ₅₀	clogP ^c	LLE ^d
5a	 H	-	 H	0.480 \pm 0.076	6.3	2.6	3.7
5b	 H	7-	 F	0.973 \pm 0.276	6.0	2.8	3.2

1 (= <i>rac</i> - 5c)		7-		0.764 ± 0.203^b	6.1	3.3	2.9
(R) - 5c		7-		0.712 ± 0.176	6.1	3.3	2.9
(S) - 5c		7-		0.489 ± 0.119	6.3	3.3	3.0
5d		7-		0.388 ± 0.080	6.4	3.3	3.1
(R) - 5d		7-		0.408 ± 0.099	6.4	3.3	3.1
(S) - 5d		7-		0.319 ± 0.066	6.5	3.3	3.2
11		7-		1.382 ± 0.394	5.9	3.2	2.7
5g		6-		3.811 ± 0.118	5.4	3.2	2.2
5h		6-		6.096 ± 0.654	5.2	3.3	1.9
5i		5-		8.042 ± 0.617	5.1	3.2	1.9
5j		7-		>10	-	3.2	-

^a IC₅₀ values were determined in an ADP Glo™ kinase assay (for details see Supporting Information (SI)).³⁶ The reported data are mean values \pm SEM from at least two independent experiments; ^b data taken from Andreev *et al.*¹²; ^c AlogP calculated with Canvas (Schrödinger LLC)³⁷; ^d Lipophilic ligand efficiency (LLE) = pIC₅₀ – clogP.³⁸

Considering these results, we next set out to resolve the binding mode of the eutomer **(S)**-**5c** to GSK-3 β by X-ray crystallography (PDB 7B6F). As we anticipated, the crystal structure confirmed interactions of the 9*H*-pyrimido[4,5-*b*]indole core to the hinge region of the kinase (Figure 1). In particular, two hydrogen-bonds were formed with the backbone of hinge residues Asp133 and Val135. Moreover, a water bridge was observed between the N-3 atom of the pyrimidine ring and Pro136, an interaction which was also suggested by our earlier MD simulations.¹² The third aromatic ring of the tricyclic core is located deeper in the pocket and the chlorine substituent is oriented towards the hydrophobic region I (HR-I) of the kinase, while the piperidine ring is accommodated in the sugar pocket. This allows the flexible cyanoethyl substituent to obtain a folded conformation under Phe67. The nitrile group displays a hydrogen bond to the side chain of Lys85. Notably, the obtained conformation of the inhibitor would be disturbed by larger substituents in the 5- or 6-position of the 9*H*-pyrimido[4,5-*b*]indole core, explaining the decreased activity of **5g-i**. The inactivity of **5j** is evident from the apparent clash caused by the methyl group in the 2-position of the pyrimidine with the protein.

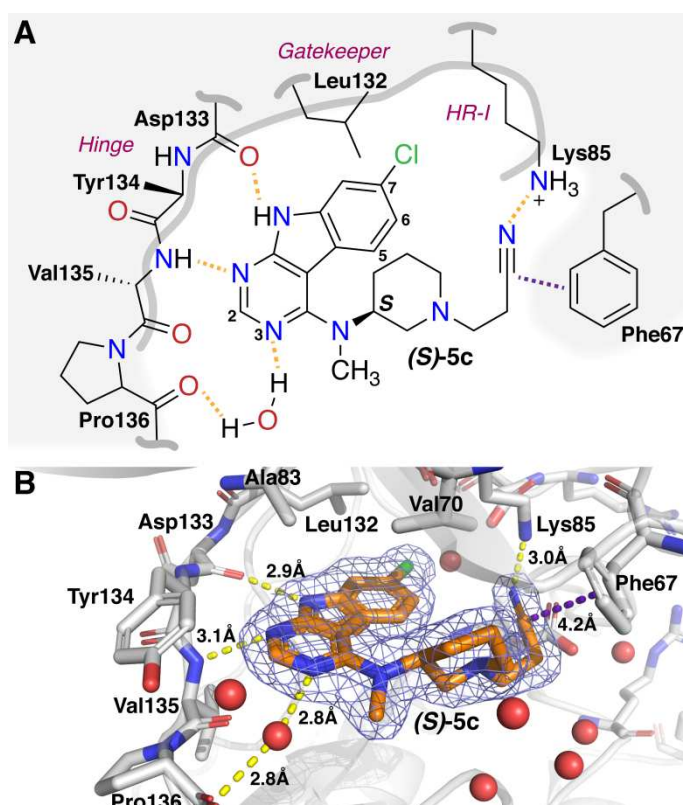


Figure 1. Co-crystal structure of (*S*)-**5c** in complex with GSK-3β (PDB 7B6F). (**A**) 2D-depiction of the observed binding mode observed in the crystal structure. (**B**) The hinge-binder of (*S*)-**5c** is stabilized by two direct and one water-bridged interaction to the protein. The chlorine atom is located near the gatekeeper residue Leu132 and the nitrile group is close proximity to Lys85. GSK-3β residues making close contacts with (*S*)-**5c** are shown in stick representation, and water molecules are displayed as red spheres. Blue mesh surface on the ligand displays a 2Fo–Fc map contoured at 1σ. Hydrogen bonds are indicated by yellow dashed lines, and distance from the Phe67 aromatic ring center to the carbon of the nitrile group is depicted as a purple dashed line.

During a closer examination of the crystal structure, we noticed that a single water molecule is trapped in the HR-I and the chlorine atom of the ligand is pointing towards it (Figure 2A). Intrigued by this finding, we decided to evaluate the solvent organization near the ligand using WaterMap.²⁴⁻²⁵ This analysis, which provides an estimate of the hydration sites and their energies, revealed both low- and high-energy hydration sites (Figure 2B, 2C). The hydration site related to the water-bridge located between the N-3 atom of the pyrimidine ring and GSK-3β was characterized as a low energy site (+0.13 kcal/mol). Importantly, we noticed that the trapped water molecule in the HR-I was indeed identified as a high-energy hydration site

(+6.71 kcal/mol). Therefore, our subsequent ligand design aimed for the displacement of this high-energy water molecule. To this end, we installed a variety of substituents at the 7-position of the 9*H*-pyrimido[4,5-*b*]indole core. Our initial efforts introducing considerably bulkier residues (**5k**, **5l**) or with a methoxy group (**5e**) resulted in compounds with decreased activity (Table 2). Also, perhaps surprisingly, the trifluoromethyl derivative (**5f**) appeared inactive. However, even the trifluoromethyl group is substantially bulkier in its radius compared to chlorine (Figure S1A, SI). Therefore, we ascertained a clear limitation on the substituent's radius in this area, most likely caused by the steric hindrance of the gatekeeper residue Leu132 (Figure 2D). We speculate that this also applied to the observed slight decrease in activity seen for derivative **11**, which carries the considerably larger iodine substituent (Figure S1A, SI). Based on these initial results, addressing this high-energy water required a long and narrow substituent. Correspondingly, we next tested a nitrile derivative (**5m**), as this moiety has been demonstrated earlier as a successful approach to displace a water molecule in the design of the autotaxin inhibitor GLPG1690 as well as Hsp90 inhibitors.³⁹⁻⁴⁰ The nitrile group is comparable to the chlorine substituent in terms of its van der Waals radius, but it is longer and reaches deeper towards the HR-I (Figure S1B, SI). Unfortunately, in this case this approach was unsuccessful as **5m** displayed even lower activity compared to the parent compound **5c**. Next, we introduced an ethynyl substituent (**15**), which is even longer than the nitrile group while maintaining a similar radius (Figure S1B, SI). To our astonishment, **15** displayed a remarkable increase in activity with an IC₅₀ value of 23 nM. Since we initially identified a trend towards (*S*)-**5c** and (*S*)-**5d** being the eutomers, we assumed that higher activity would be observed for the corresponding stereoisomer of **15**. Indeed, compound (*S*)-**15** displayed an improved IC₅₀ value of 6 nM.

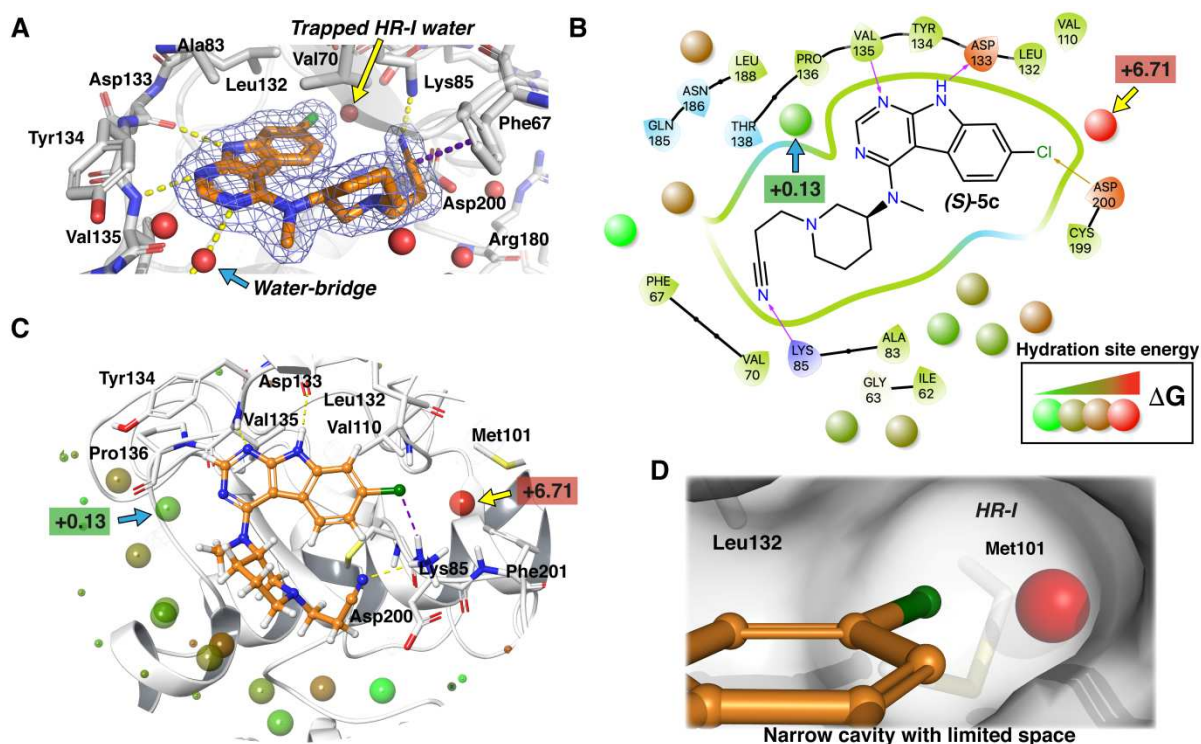
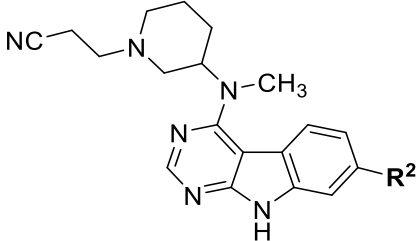
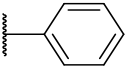
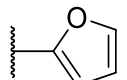
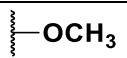
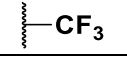
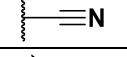
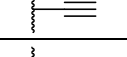
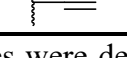


Figure 2. The WaterMap analysis of the GSK-3β-(S)-5c crystal structure revealed a high-energy water in the HR-I region. **(A)** In the crystal structure, a trapped water molecule was found in the HR-I region (indicated by a yellow arrow). The water molecule which forms the water bridge is indicated by a blue arrow. **(B)** 2D- and **(C)** 3D-depiction of the WaterMap analysis. The hydration site related to the water bridge was identified as a low-energy site (+0.13 kcal/mol), whereas the estimated free energy for the trapped water molecule in HR-I is high (+6.71 kcal/mol). All other hydration sites near the ligand located in the solvent interface displayed low or medium energy values. **(D)** The chlorine atom of (S)-5c is pointing towards the HR-I, where the high-energy water molecule is located. The gatekeeper residue Leu132 sterically restricts the access of the ligand to the HR-I.

Table 2. Structures and biological activities of compounds addressing the high-energy water molecule.

					
No.	R ²	GSK-3β IC ₅₀ ± SEM [μM] ^a	pIC ₅₀	clogP ^b	LLE ^c
5k		5.112 ± 0.270	5.3	4.1	1.2
5l		5.299 ± 0.145	5.3	3.3	2.0
5e		8.690 ± 0.057	5.1	2.6	2.5
5f		> 10	-	3.5	-
5m		1.204 ± 0.146	5.9	2.5	3.4
15		0.023 ± 0.008	7.6	3.7	3.9
(S)-15		0.006 ± 0.003	8.2	3.7	4.5

^a IC₅₀ values were determined in an ADP Glo™ kinase assay.³⁶ The reported data are mean values ± SEM from at least two independent experiments; ^b AlogP calculated with Canvas (Schrödinger LLC)³⁷; ^c LLE = pIC₅₀ – clogP.³⁸

We were puzzled about the remarkable activity differences among the ethinyl (**15**) and the nitrile (**5m**) derivatives. To further rationalize this finding, we ran additional WaterMap analyses for both compounds, using them as ligands in the simulations. Interestingly, with the nitrile (**5m**) the high-energy hydration site appeared at the same location as with (**S**)-**5c**, whereas this hydration site was shifted with the highly active ethinyl analog (**S**)-**15** (Figure S2, SI). These results demonstrated that adequate length of the ethinyl substituent was required to push the water, with the nitrile group being “too short” in this case. The evaluated energy for this hydration site for with the nitrile substituent harboring **5m** (+6.21 kcal/mol, calculated for the *S*-enantiomer) was comparable with the chlorine substituted (**S**)-**5c** (+6.71 kcal/mol). Even though the electrostatic potential among these compounds was notably different in their high-energy water facing apical site (Figure S3, SI), no interactions between the water molecule and

the ligand were observed. Therefore, the decreased biological activity of **5m** most likely arose from its lower lipophilicity (see LLE in Table 2). For the shifted hydration site with **(S)-15**, however, even higher energy (+7.97 kcal/mol) was estimated by the WaterMap. Therefore, this approach failed to provide us further rationale for the remarkable activity of **(S)-15**.

To further investigate the water molecule's behavior in the high-energy site, we conducted 10 x 1 μ s MD simulations for both compounds, **(S)-5c** and **(S)-15**, in complex with GSK-3 β . Throughout the simulations the two inhibitors displayed nearly identical interaction patterns, demonstrating that the ethynyl substituent does not affect the direct interactions of the ligand with GSK-3 β (Figure S4, SI). Comprehensive protein sidechain conformational sampling occurs within a microsecond timescale;⁴¹ therefore, these simulations would be expected to reveal the putative water displacement if it occurred. Interestingly, these longer simulations agreed with the notably shorter (2 ns) WaterMap simulations: the water molecule was slightly shifted but not displaced from the HR-I site. We further evaluated the water location as well as the solvent exposure of the lipophilic residue sidechains in this region. There were in total five lipophilic residues found in this area: gatekeeper Leu132 and Val110 that were in close contact with the ligand, Leu112 and Leu130 located deep in the pocket, and Met101 protruding from the α C-helix (Figure 3A). Leu132 was almost fully shielded from the solvent exposure by **(S)-15**, which clearly pushed the water molecule away from the gatekeeper (Figure 3B, 3C). A similar trend was also evident in the case of Val110, while only marginal changes were observed for the other lipophilic residues. There is virtually no change in the water exposure of Leu112 with **(S)-15**. Met101 appeared somewhat less exposed to water with **(S)-15**, whereas a slight increase in the water exposure of Leu130 was observed. These findings clearly demonstrated that the hydration site was shifted away from the gatekeeper Leu132, but the water molecule remained in the HR-I (Figure 3D). Next, we wanted to re-evaluate the energy of this shifted high-energy hydration site. To this end, we selected five conformations

(at 1 μ s) of the **(S)-15** MD simulations. Of note, one should always use caution when applying WaterMap for an MD simulation derived structure, as the method has been originally developed to be applied for crystal structures and is highly sensitive to changes in sidechain conformations. In other words, the thermodynamic quantities calculated by WaterMap only apply to the input conformation. Intriguingly, even though the slightly shifted water molecule was still trapped in the hydrophobic environment, WaterMap now demonstrated significantly decreased energy of this hydration site, which is mainly enthalpy driven (Figure 3F). We noticed that the subtle shift in the position of the water molecule resulted in altered hydrogen bond interactions with the protein (specifically the loss of the hydrogen bond to Asp200) (Figure 3E, Figure S5, SI). As a consequence, this shift appears to improve hydrogen bonding with Phe201 and Glu97, which provides an explanation for the observed decrease in the hydration site energy. The estimated hydration site energy (average difference of 2.302 kcal/mol compared to **(S)-5c**) was in line with the observed biological activities, as a free energy difference of 2.6 kcal/mol would be expected in their binding affinity (80-fold difference).

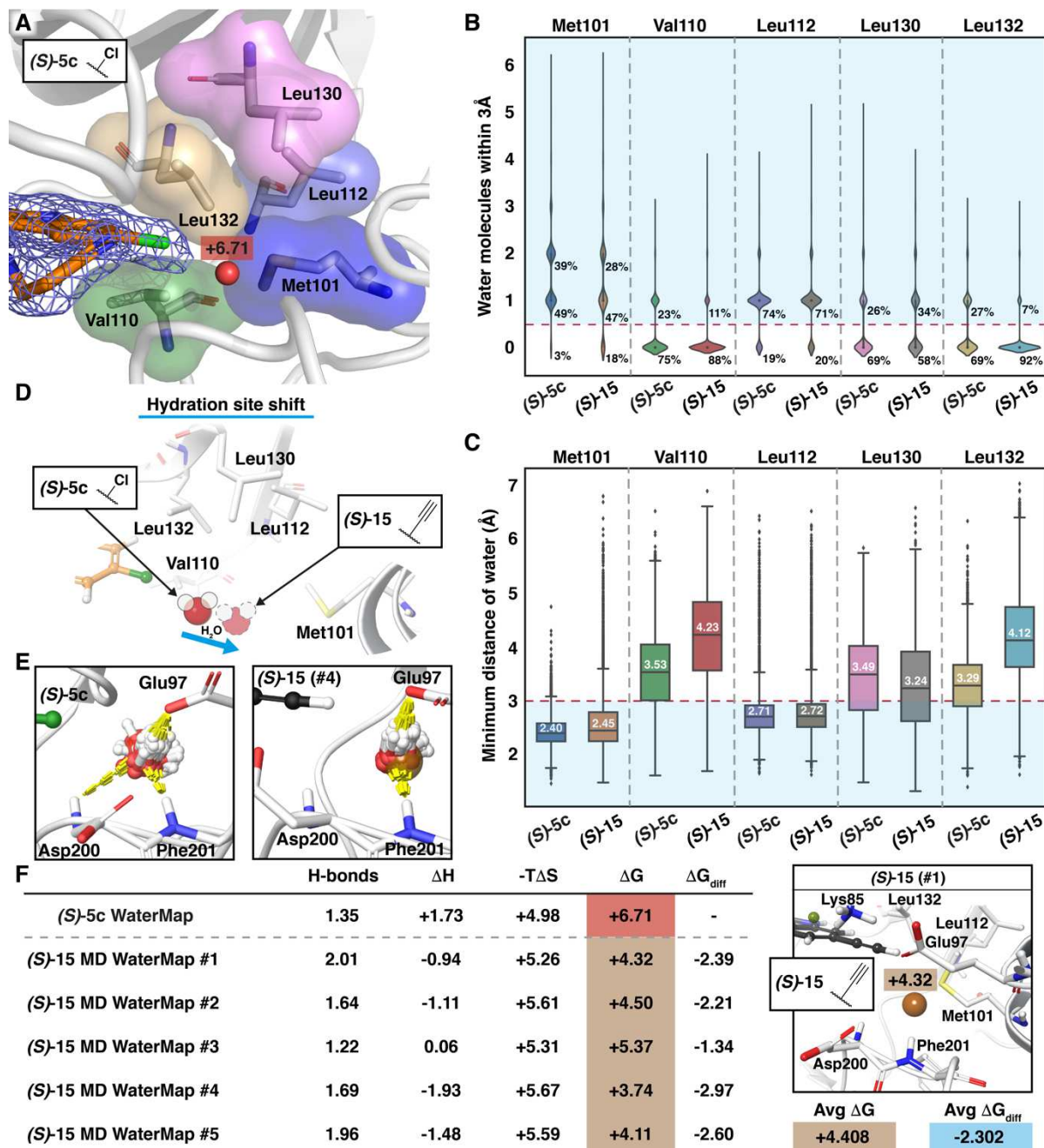
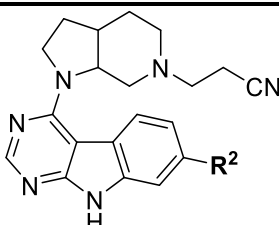
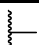
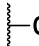
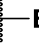
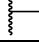
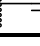


Figure 3. Molecular dynamics simulations reveal the high-energy hydration site shift that is accompanied with decreased energy. **(A)** Lipophilic residues Met101, Val110, Leu112, Leu130 and Leu132 are flanking the high-energy water in the HR-I. **(B)** Quantitation of the observed water molecules within 3Å of the sidechains of the selected lipophilic residues during the simulations (a total simulation time of 10 μ s for each ligand). Light-blue shaded area indicates water exposure of the lipophilic sidechains. **(C)** Observed minimum distance of water to the sidechain of the selected lipophilic residues during the simulations. Light-blue shaded area indicates water exposure of the lipophilic sidechains. In the boxplots, the box indicates quartiles of the dataset (25–75%) and whiskers the rest of the data within 1.5 times the interquartile range (IQR) (outliers are shown with black diamonds). Median values are provided as horizontal lines in the boxes. **(D)** Schematic depiction of the hydration site movement based on the data in **B** and **C**. **(E)** Based on WaterMap simulations, the subtle shift of the water molecule's location induces alterations in the hydrogen bond network of the high-energy water molecule (see also Figure S5, SI). **(F)** The WaterMap analysis of the MD simulation output

structures for five replicas of **(S)**-**15** demonstrate that the shifted hydration site has lower energy compared to **(S)**-**5c**.

To examine if our earlier successful rigidification approach on this compound series also applies here (Scheme 1), we evaluated a set of rigidified congeners (Table 3). Indeed, most of these compounds displayed enhanced IC₅₀ values compared to their nonrigid counterparts. Importantly, the ethynyl derivative **22** exhibited outstanding potency (IC₅₀ value of 2 nM), confirming the highly beneficial effect of this substituent. We also observed a clear trend of enhanced activity alongside the increasing size of the halogens (**2**, **19-21**). The results of this rigidified compound set imply a similar impact of the substituent in the 7-position on the high-energy hydration site as observed with the nonrigid analogs.

Table 3. Structures and biological activities of rigid compounds.

						
No.	R ²	GSK-3β IC ₅₀ ± SEM [μM] ^a	(IC ₅₀ nonrigid)	pIC ₅₀	clogP ^d	LLE ^e
19		2.668 ± 1.488	(0.973)	5.6	2.7	2.9
2		0.130 ± 0.008 ^b	(0.764 ^b)	6.9	3.2	3.7
20		0.066 ± 0.015	(0.388)	7.2	3.2	3.9
21		0.132 ± 0.036	(1.382)	6.9	3.1	3.8
22		0.002 ± 0.000	(0.023)	8.7	3.6	5.1

^a IC₅₀ values were determined in an ADP Glo™ kinase assay.³⁶ The reported data are mean values ± SEM from at least two independent experiments. ^b data taken from Andreev *et al.*¹², ^c IC₅₀ values of the corresponding non-rigid compounds from Tables 1 and 2; ^d AlogP calculated with Canvas (Schrödinger LLC)³⁷; ^e LLE = pIC₅₀ – clogP.³⁸

Next, we set out to evaluate the cellular target engagement of **(S)**-**5c**, **(S)**-**15**, **20** and **22**. In a NanoBRET assay, these inhibitors generally demonstrated GSK-3β binding affinities in the single-digit micromolar range (for details see SI and Table S1, SI). Importantly, this data

correlates well with the IC₅₀ values determined in the kinase activity assay with **(S)-15** displaying the highest affinity to GSK-3 β in cells.

These results motivated us to further characterize **(S)-15** along with **20** in terms of their intracellular GSK-3 inhibition and neuroprotective effects in neuronal SH-SY5Y cells. The treatment of SH-SY5Y cells with **(S)-15** and **20** at concentrations lower than 10 μ M and 20 μ M, respectively, did not affect cell viability (3-(4,5-dimethylthiazol-2-yl)-2,5-diphenyltetrazolium bromide (MTT) assay (Figure S6, SI).⁴² Therefore, we selected the concentration of 5 μ M to perform an immunoblotting assay monitoring the phosphorylation status of GSK-3 in the presence of the inhibitors. While both **(S)-15** and **20** increased the phospho-GSK-3 α/β (Ser21/9) (inactive GSK-3 α/β form), only **(S)-15** decreased the phospho-GSK-3 α/β (Tyr279/Tyr216) (active GSK-3 α/β form), after 3 h of treatment in neuronal SH-SY5Y cells (Figure S7, SI). As Tyr279 and Tyr216 are autophosphorylation sites of GSK-3 α and GSK-3 β , respectively, the phosphorylation status of these residues reflects the enzymatic activity of the kinase.⁴³⁻⁴⁵ Accordingly, these results demonstrate that **(S)-15** inhibits GSK-3 activity in cells targeting the ATP binding pocket of both GSK-3 α and GSK-3 β and rendering its inhibition selective and persistent. Furthermore, we investigated the neuroprotective effects of **(S)-15** and **20** against the neurotoxicity induced by hydrogen peroxide (H₂O₂, 100 μ M), that mimics general oxidative stress.⁴⁶ The concomitant treatment of the SH-SY5Y cells with H₂O₂ and the compounds (5 μ M) significantly decreased the neurotoxicity elicited by oxidative stress on a neuronal level (Figure S8, SI). Interestingly, the neuroprotective effect of **(S)-15** was significantly higher than of **20** corroborating the ability of **(S)-15** to promote the neuronal survival through the strong inhibition of GSK-3 β .

Finally, to assess the kinome selectivity of the inhibitors **(S)-15** and **22**, we evaluated their biological activity on a subset of 57 kinases. At an inhibitor concentration of 500 nM only few kinases were substantially inhibited by **(S)-15** and **22** (Figure 4; see full list in Table S2, SI). These data suggested a similar off-target profile for these two compounds. Notably, the

more potent rigid inhibitor **22** consistently exhibited stronger inhibition on all off-target kinases compared to its non-rigid counterpart (**S**)-**15**. Even though the off-targets appeared only remotely related, they share structural similarities in residues near the HR-I that participate in the accommodation of the ethynyl substituent in the 7-position of the 9*H*-pyrimido[4,5-*b*]indole core (Figure 4C). In particular, they mostly harbor a branched gatekeeper residue (Ile, Leu, Thr and Val) as well as a large lipophilic amino acid protruding from the α C helix (Met, Leu and Phe). Thus, we anticipate that these residues together with a suitable overall binding site topology allow binding of (**S**)-**15** or **22**, offering a putative explanation to the observed off-target activity.

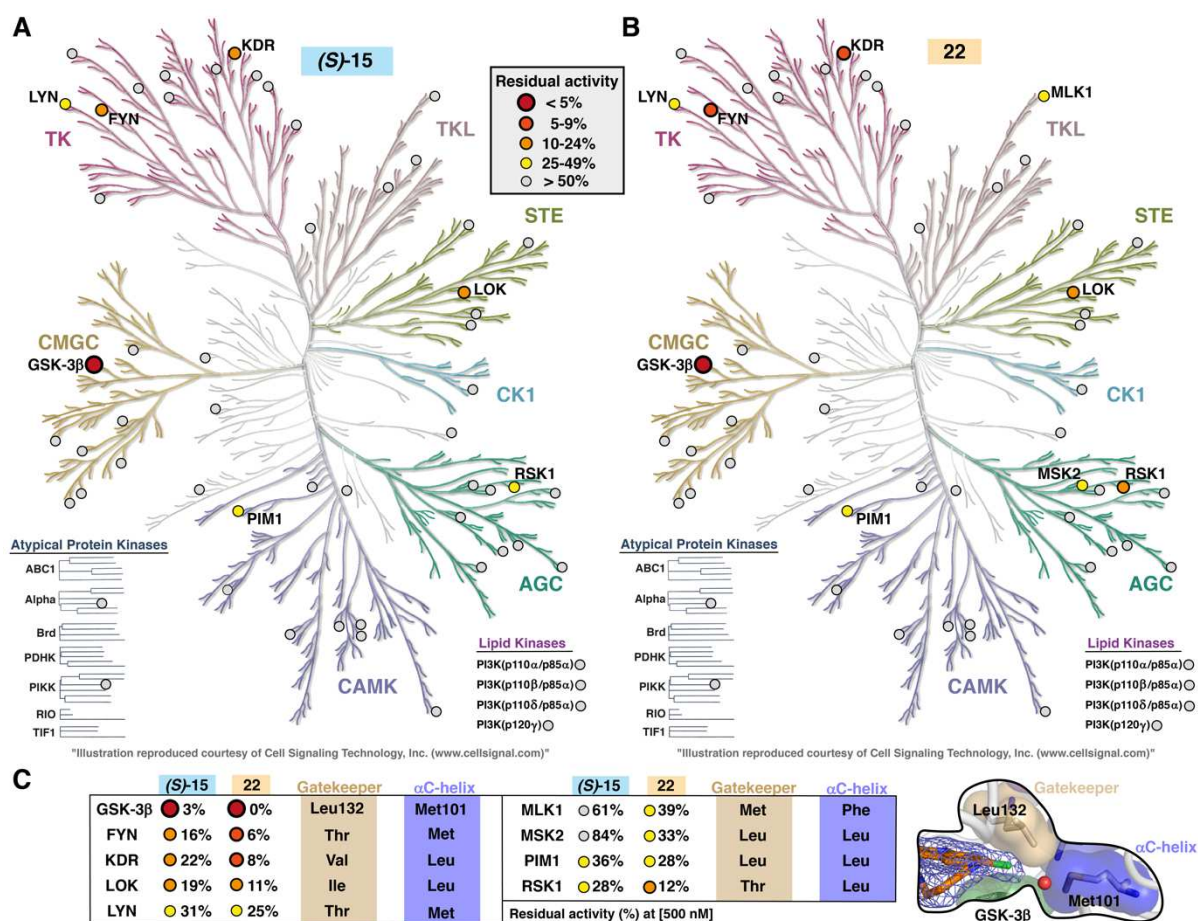
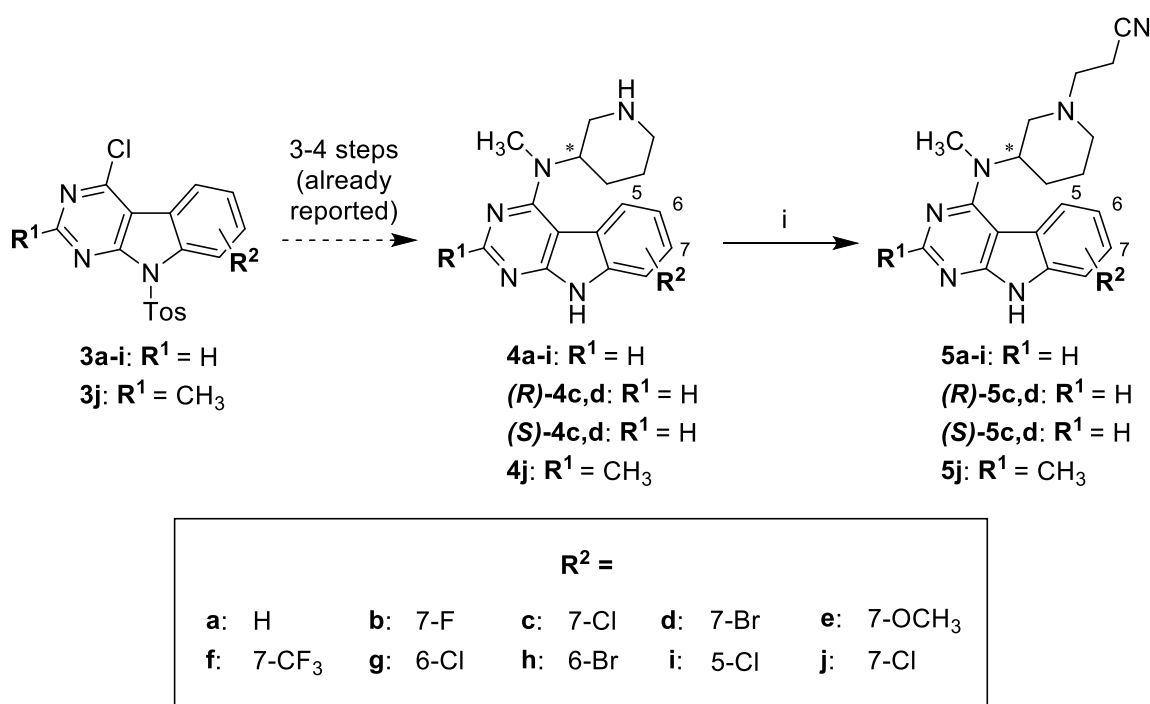


Figure 4. Selectivity of the (**S**)-**15** and **22** within the human kinome. (A) Selectivity of compound (**S**)-**15**. All tested kinases are highlighted with circles and colored according to their residual activity at 500 nM inhibitor concentration. (B) Selectivity of compound **22**. (C) The residual activities of the off-targets which display <50% residual activity for (**S**)-**15** or **22**. The corresponding gatekeeper and α C-helix residues are listed for each kinase. The figures A and B were generated with the help of the KinMap.⁴⁷

Chemistry

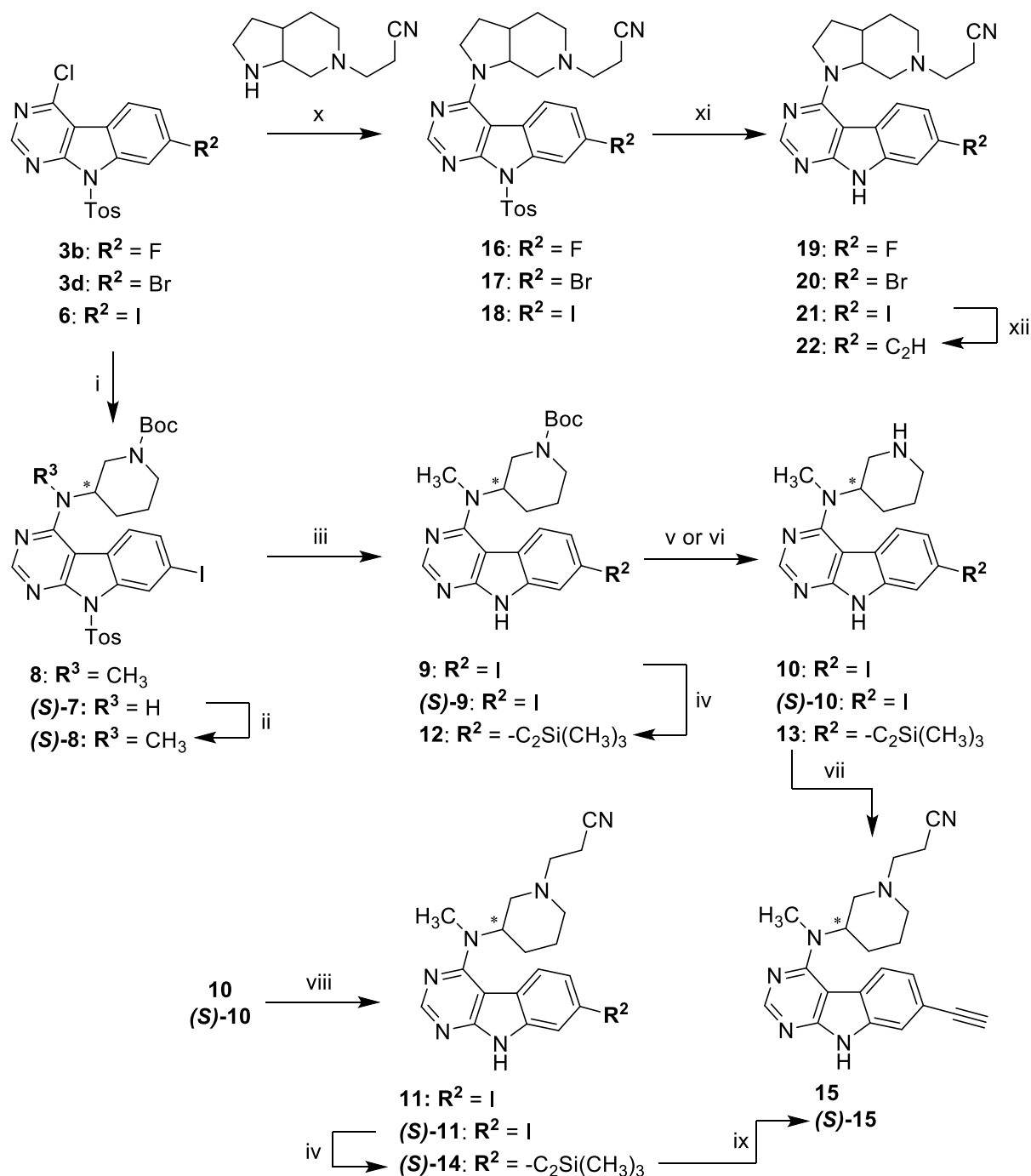
We recently reported the synthetic preparation of piperidines **4a-j** and the enantiopure analogs (*R*)-**4c,d** and (*S*)-**4c,d** from 9-tosyl-9*H*-pyrimido[4,5-*b*]indoles **3a-j** (Scheme 2).³⁵ These piperidine intermediates display diverse substitution patterns of the tricyclic core and served as precursors to prepare the final compounds **5a-j** as well as (*R*)-**5c,d** and (*S*)-**5c,d** within the herein reported study. As previously described in the synthesis of inhibitor **1**, the cyanoethyl substituent was installed on the piperidine nitrogen by Michael reaction with acrylonitrile.¹²



Scheme 2. Synthetic route towards compounds **5a-j** and the enantiopure analogs (*R*)-**5c,d** and (*S*)-**5c,d** listed in Tables 1 and 2. Reagents and conditions: (i) acrylonitrile, MeOH, rt (37-84%).

Moreover, our established synthetic methodologies were successfully applied to the corresponding 7-iodine derivatives (Scheme 3).³⁵ In detail, previously reported 7-iodo-9-tosyl-9*H*-pyrimido[4,5-*b*]indole (**6**) was reacted with *N*-Boc-3-(methylamino)piperidine in a nucleophilic aromatic substitution (S_NAr) giving intermediate **8**. In case of the enantiopure analog (*S*)-**8**, commercially available (*S*)-*N*-Boc-3-aminopiperidine was used in the S_NAr resulting in (*S*)-**7**, which was subsequently methylated with iodomethane under strictly anhydrous basic conditions. Intermediates **8** and (*S*)-**8** were then subjected to deprotection

procedures to generate piperidines **10** and (*S*)-**10**, which were similarly reacted with acrylonitrile to form final compound **11** and intermediate (*S*)-**11**.



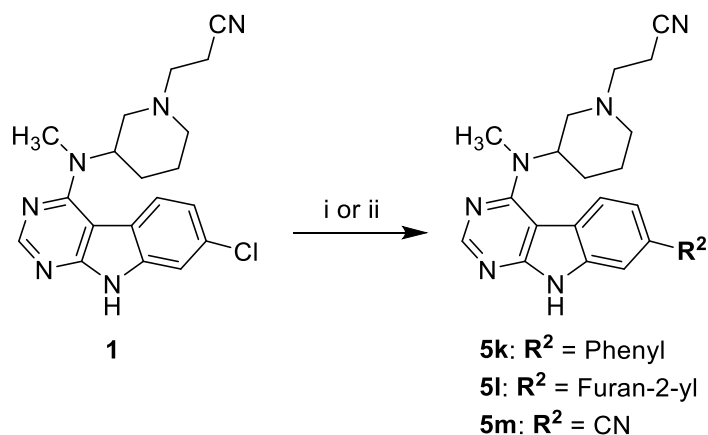
Scheme 3. Synthetic route towards compounds **11**, **15**, (*S*)-**15** and **19-21** listed in Tables 2 and 3. Reagents and conditions: (i) **6**, DIPEA, DMF, 70 °C (54% for (*S*)-**7**); (ii) iodomethane, NaH, DMF, -10 °C to rt (5); (iii) *K*tBuO, THF, rt (54-58% over two steps); (iv) TMS-acetylene, Pd(PPh₃)₄ or PdCl₂(PPh₃)₂, CuI, TEA, DMF, rt or 50 °C (86-96%); (v) **9** or (*S*)-**9**, TFA, DCM, rt (quant.); (vi) **12**, 4N HCl in 1,4-dioxane, rt (42%); (vii) (1) acrylonitrile, MeOH, rt, (2)

K₂CO₃, MeOH, rt (41% over two steps); (viii) acrylonitrile, MeOH, rt (44-74%); (ix) K₂CO₃, MeOH, rt (68%); (x) DIPEA, DMF, 70 °C (41-62%); (xi) K^tBuO, THF, rt (40-62%); (xii) (1) TMS-acetylene, PdCl₂(PPh₃)₂, CuI, TEA, DMF, rt, (2) K₂CO₃, MeOH, rt (41% over two steps).

For the synthesis of the racemic ethynyl derivative **15**, a Sonogashira cross coupling reaction was initially performed with the Boc-protected intermediate **9** and trimethylsilylacetylene (TMS-acetylene) following a modified literature protocol (Scheme 3).⁴⁸ The treatment of the Sonogashira product **12** with TFA in DCM, however, resulted in simultaneous Boc and TMS deprotection along with pronounced by-product formation. While the application of 4N HCl in 1,4-dioxane allowed for a selective Boc cleavage, it still suffered from a poor yield in the synthesis of **13**. Nevertheless, this intermediate was converted into the racemic final compound **15** in a one-pot two-step reaction, including introduction of the cyanoethyl substituent followed by TMS deprotection with K₂CO₃.

In order to avoid an acidic Boc deprotection in presence of the alkyne substituent in the synthesis of the *S*-configured analog (**S**)-**15**, the Pd-catalyzed alkynylation was instead carried out with (**S**)-**11**. The TMS protecting group of (**S**)-**14** was then smoothly cleaved with K₂CO₃ to obtain (**S**)-**15** in a 2.5-fold higher yield over four steps compared to the initial approach.

Compounds **5k-l** bearing a nitrile substituent or aryl moieties in the 7-position of the 9*H*-pyrimido[4,5-*b*]indole core were prepared by cross coupling reactions from the already reported compound **1** (Scheme 4). In the case of **5m**, precursor **1** was subjected to a palladium-catalyzed cyanation procedure using K₄[Fe(CN)₆] as cyanide source,⁴⁹ whereas **5k** and **5l** were synthesized *via* Suzuki coupling with the appropriate aryl boronic acids applying common procedures.



Scheme 4. Synthetic route towards compounds **5k-m** listed in Table 2. Reagents and conditions: (i) $\text{K}_4[\text{Fe}(\text{CN})_6] \cdot 3\text{H}_2\text{O}$, BrettPhos Pd G3, BrettPhos, KOAc, 1,4-dioxane: H_2O (1:1, v/v), 100 °C (26%); (ii) appropriate aryl boronic acid, XPhos Pd G3, K_3PO_4 , 1,4-dioxane: H_2O (4:1, v/v), 100 °C (60-66%).

The rigidized compounds **19-21** were accessible by a two-step synthetic route starting from the corresponding 9-tosyl-9*H*-pyrimido[4,5-*b*]indoles **3b**, **3d** and **6** (Scheme 3). The required 3-(octahydro-6*H*-pyrrolo[2,3-*c*]pyridin-6-yl)propanenitrile building block was prepared as described previously and introduced under $\text{S}_{\text{N}}\text{Ar}$ conditions.¹² Application of the tosyl deprotection protocol on intermediates **16-18** eventually furnished **19-21**. In addition, the iodine derivative **21** was subjected to the established methodology to introduce the ethynyl substituent to afford inhibitor **22**. We previously resolved the molecular structure of **2** by X-ray crystallography, confirming that the protocols for the preparation of the 3-(octahydro-6*H*-pyrrolo[2,3-*c*]pyridin-6-yl)propanenitrile building block and its use in the subsequent steps deliver a mixture of the (3*aR*, 7*aS*) and (3*aS*, 7*aR*) enantiomers of the respective final compound.¹²

Conclusion

We utilized a newly obtained co-crystal structure of the moderately potent GSK-3 β inhibitor (*S*)-**5c** to identify highly potent compounds. The binding affinity of these compounds was

improved by addressing a trapped high-energy water molecule in the HR-I. Here, the ethynyl substituent proved highly beneficial, affording an up to 80-fold increase in potency. The improved inhibitory activity of **(S)-15** towards GSK-3 β (IC₅₀ value of 6 nM) translated also into a cellular context, as the target engagement was demonstrated in a NanoBRET assay together with the neuroprotective effects against H₂O₂ and reduced autophosphorylation of GSK-3 in neuronal SH-SY5Y cells. In addition, the ethynyl substituted compounds displayed favorable kinome selectivity profiles.

Based on our MD simulations and WaterMap analysis, this ethynyl substituent induced only a subtle shift in the position of the trapped water molecule, which resulted in a decreased energy of the hydration site that is in line with the observed biological activity. This decrease in energy was mainly driven by enthalpy, arising from alterations in the protein–water hydrogen bond network. The nearly identical interactions of **(S)-5c** and **(S)-15** to GSK-3 β and improved LLE values of the ethynyl derivatives suggested that it is mainly the subtle change in the high-energy hydration site location that influences the ligand binding. To the best of our knowledge, these results demonstrate for the first time that a high-energy water does not necessarily need to be fully displaced, replaced or interacted by the ligand to alter its energy in a beneficial manner for the ligand binding. In the location where the high-energy water molecule was found protein kinases harbor conserved water molecules, which are commonly interacted with by type I inhibitors.⁵⁰ This also applies to human GSK-3 β , based on our analysis of the high-resolution crystal structures currently available in the Protein Data Bank in Europe (PDBe) (for full list, see csv-file, SI). Interestingly, in a completely different compound series we observed that stabilizing a dynamic water network and avoiding unfavorable water exposure related to the HR-I of GSK-3 β is also crucial for the inhibitor activity.⁵¹

We noted that a combination of longer (μ s) MD simulations with the short (ns) and restrained WaterMap simulations is required for a more accurate analysis of the energy evaluation of a shifted hydration site (see workflow of the combination approach in Figure S9,

SI). To note, there are always limitations and inaccuracies associated with in silico techniques, especially related to the description of the solvent; nevertheless, the herein applied methodology proved highly efficient, highlighting the relevance of water-guided in silico approaches for the ligand design process. Overall, these results highlight the importance of considering even subtle changes of hydration site positions in the ligand design process.

Experimental

Chemistry

General information

All solvents and reagents were obtained from commercial sources and utilized without additional purification. Solvents used for analytical chromatography were of HPLC grade. 3-(octahydro-6*H*-pyrrolo[2,3-*c*]pyridin-6-yl)propanenitrile was prepared according to modified reported procedures and obtained as free base or TFA salt.¹² High performance liquid chromatography (HPLC) was carried out on an HP1090 series II HPLC system from Hewlett-Packard (Palo Alto, CA, USA) or an 1100 series HPLC system from Agilent Technologies (Santa Clara, CA, USA). The systems consisted of a binary pump, a column compartment equipped with a Luna C8(2) 100 Å RP column (4.6 mm inner diameter × 150 mm length, 5 µm particle size) from Phenomenex (Torrance, CA, USA), an autosampler and a diode array detector (DAD) (purity of test compounds determined at 254 nm). The mobile phases A (MeOH) and B (aqueous 0.01M KH₂PO₄ buffer, pH 2.3) were used in the following gradient: mobile phase A 40% to 85% during 8 min, mobile phase A 85% constant for 5 min, mobile phase A 85% to 40% during 1 min, mobile phase A 40% constant for 2 min; complete run time 16 min; flow rate 1.5 mL/min. Sample injection volume was 5 µL.

Chiral chromatographic analysis was performed on a 1290 Infinity series LC system from Agilent Technologies (Santa Clara, CA, USA). The system consisted of a binary pump, a

thermostatted column compartment equipped with a Chiralpak IB-U column (3.0 mm inner diameter x 100 mm length, 1.6 μ m particle size) from Daicel (Osaka and Tokyo, Japan), an autosampler and a DAD (chiral purity of test compounds determined at 254 nm). To minimize extra column volume, the system was provided with an ultralow dispersion kit (including a Max-Light ultralow dispersion cartridge flow cell with an inner volume of 0.6 μ L, an ultralow dispersion needle seat and capillaries with 0.075 mm inner diameter from autosampler to column compartment (350 mm length) and from column compartment to DAD (220 mm length)). The mobile phase was composed of 90% n-heptane, 10% isopropanol and 0.1% diethylamine, flow rate 0.15 mL/min. Samples were prepared by diluting 10 mM aliquotes in DMSO by the factor 10 with the mobile phase to a total concentration of 1 mM and injected with a volume of 5 μ L. The enantiomeric excess (ee) of the enantiopure final compounds was >98% in all cases.

Thin layer chromatography (TLC) was carried out on TLC Silica gel F254 sheets from Merck (Darmstadt, Germany) or Alugram Sil G/UV254 sheets from Macherey-Nagel (Düren, Germany). Bands were visualized under UV light at 254 nm.

Electrospray ionization mass spectrometry (ESI-MS) was performed on an Advion expressions CMS TLC-ESI-MS coupling system from Advion (Ithaca, NY, USA) operating in positive ESI mode (capillary temperature 250 °C, capillary voltage 180 V, source gas temperature 250 °C, ESI voltage 3500 V) and negative ESI mode (capillary temperature 250 °C, capillary voltage 180V, source gas temperature 250 °C, ESI voltage 2500 V), elution with LCMS grade MeOH.

Flash column chromatography was performed on a Puriflash 430 or XS 420 from Interchim (Montluçon, France) on Davisil Chromatographic Silica Media LC60A (20–45 μ m) from Grace Davison Discovery Sciences (MD, USA) or Interchim Puriflash prepacked silica columns (SIHP-JP, 30 μ m) from Interchim (Montluçon, France) and Geduran Si60 63200 μ m silica gel

from Merck (Darmstadt, Germany) for pre-column preparation. Mobile phases are described in the detailed procedures for each purified compound.

Nuclear magnetic resonance (NMR) analysis was carried out on 200, 300, and 400 MHz Avance and 400 MHz Ascend spectrometers from Bruker (Billerica, MA, USA). Spectra were calibrated to residual peaks of utilized solvents. The chemical shifts are reported in parts per million (ppm) relative to tetramethylsilane ($\delta = 0$).

Experimental procedures

*General Procedure A for the preparation of final compounds **5a,b** and **5d-j** and the enantiopure analogs (**R**)-**5c,d** and (**S**)-**5c,d***

The appropriate secondary amine intermediate was dissolved in MeOH (HPLC grade or dry) and acrylonitrile was added. The mixture was stirred at rt and under N₂ atmosphere for 16 h and concentrated under reduced pressure. The residue was purified by flash column chromatography.

*Detailed procedures for the preparation of final compounds **5a,b** and **5d-j** and the enantiopure analogs (**R**)-**5c,d** and (**S**)-**5c,d***

3-(3-(Methyl(9H-pyrimido[4,5-*b*]indol-4-yl)amino)piperidin-1-yl)propanenitrile (5a**)**

The title compound was prepared from *N*-methyl-*N*-(piperidin-3-yl)-9H-pyrimido[4,5-*b*]indol-4-amine (36.0 mg, 0.13 mmol) and acrylonitrile (10.1 mg, 0.19 mmol) in dry MeOH (5 mL) according to general procedure A. Purification by flash column chromatography (SiO₂; DCM:EtOH gradient elution from 98:2 to 9:1) gave 26 mg (61% yield); ¹H NMR (400 MHz, DMSO-*d*₆) δ 12.07 (s, 1H), 8.39 (s, 1H), 7.80 (d, *J* = 8.0 Hz, 1H), 7.48 (d, *J* = 7.8 Hz, 1H), 7.39

(t, $J = 7.5$ Hz, 1H), 7.33 – 7.27 (m, 1H), 4.52 – 4.41 (m, 1H), 3.15 (s, 3H), 3.07 – 2.99 (m, 1H), 2.90 – 2.80 (m, 1H), 2.73 – 2.66 (m, 2H), 2.65 – 2.58 (m, 2H), 2.41 – 2.34 (m, 1H), 1.99 – 1.90 (m, 1H), 1.86 – 1.67 (m, 3H), 1.57 – 1.44 (m, 1H); ^{13}C NMR (101 MHz, DMSO- d_6) δ 159.6, 157.0, 153.4, 136.6, 124.7, 122.5, 120.5, 120.0, 119.5, 111.2, 97.6, 55.7, 54.8, 53.0, 52.2, 32.5, 27.3, 24.4, 14.9; ESI-MS: (m/z) 335.1 $[\text{M}+\text{H}]^+$, 357.0 $[\text{M}+\text{Na}]^+$, 333.0 $[\text{M}-\text{H}]^-$; HPLC *method B*: $t_r = 2.391$ min.

3-(3-((7-Fluoro-9*H*-pyrimido[4,5-*b*]indol-4-yl)(methyl)amino)piperidin-1-yl)propanenitrile
(5b)

The title compound was prepared from 7-fluoro-*N*-methyl-*N*-(piperidin-3-yl)-9*H*-pyrimido[4,5-*b*]indol-4-amine (80.0 mg, 0.27 mmol) and acrylonitrile (28.1 mg, 0.53 mmol) in dry MeOH (7 mL) according to general procedure A. Purification by flash column chromatography (SiO₂, DCM:EtOH gradient elution from 98:2 to 9:1) gave 44 mg (47% yield); ^1H NMR (400 MHz, DMSO- d_6) δ 12.21 (s, 1H), 8.38 (s, 1H), 7.78 (dd, $J = 8.8, 5.3$ Hz, 1H), 7.24 (dd, $J = 9.4, 2.4$ Hz, 1H), 7.15 (td, $J = 9.4, 2.4$ Hz, 1H), 4.50 – 4.35 (m, 1H), 3.13 (s, 3H), 3.09 – 3.02 (m, 1H), 2.90 – 2.81 (m, 1H), 2.74 – 2.66 (m, 2H), 2.65 – 2.58 (m, 2H), 2.42 – 2.33 (m, 1H), 1.99 – 1.89 (m, 1H), 1.81 – 1.65 (m, 3H), 1.55 – 1.42 (m, 1H); ^{13}C NMR (101 MHz, DMSO- d_6) δ 160.2 (d, $J = 239.8$ Hz), 159.3, 157.6, 153.2, 137.4 (d, $J = 12.6$ Hz), 123.9 (d, $J = 10.0$ Hz), 120.0, 116.3, 108.3 (d, $J = 23.5$ Hz), 97.7 (d, $J = 26.0$ Hz), 97.3, 55.7, 54.8, 53.0, 52.2, 32.5, 27.2, 24.3, 15.0; ESI-MS: (m/z) 353.2 $[\text{M}+\text{H}]^+$, 375.2 $[\text{M}+\text{Na}]^+$, 351.1 $[\text{M}-\text{H}]^-$; HPLC *method B*: $t_r = 2.804$ min.

(*R*)-3-(3-((7-Chloro-9*H*-pyrimido[4,5-*b*]indol-4-yl)(methyl)amino)piperidin-1-yl)propanenitrile (**(*R*)-5c**)

(*R*)-7-chloro-*N*-methyl-*N*-(piperidin-3-yl)-9*H*-pyrimido[4,5-*b*]indol-4-amine (50.0 mg, 0.16 mmol) and acrylonitrile (12.6 mg, 0.24 mmol) were stirred in dry MeOH (15 mL) at rt and

under N₂ atmosphere for 6 h. DIPEA (24.6 mg, 0.19 mmol) was added to promote conversion and stirring continued overnight. The mixture was concentrated under reduced pressure. The residue was dissolved in DCM and the solution washed with saturated NH₄Cl solution (3 x 10 mL), dried over Na₂SO₄ and concentrated under reduced pressure. Purification of the residue twice by flash column chromatography (SiO₂, DCM:MeOH gradient elution from 95.5:4.5 to 93.5:6.5 and SiO₂, DCM:EtOH gradient elution from 1:0 to 93:7) gave 30 mg of a white solid (51% yield); ¹H NMR (400 MHz, DMSO-*d*₆) δ 12.22 (s, 1H), 8.40 (s, 1H), 7.78 (d, *J* = 8.7 Hz, 1H), 7.48 (d, *J* = 2.0 Hz, 1H), 7.34 (dd, *J* = 8.6, 2.0 Hz, 1H), 4.52 – 4.40 (m, 1H), 3.14 (s, 3H), 3.11 – 3.03 (m, 1H), 2.91 – 2.82 (m, 1H), 2.76 – 2.69 (m, 2H), 2.66 – 2.59 (m, 2H), 2.43 – 2.34 (m, 1H), 2.02 – 1.89 (m, 1H), 1.82 – 1.66 (m, 3H), 1.57 – 1.42 (m, 1H); ¹³C NMR (101 MHz, DMSO-*d*₆) δ 159.4, 157.4, 153.8, 137.4, 129.2, 123.9, 120.7, 120.1, 118.6, 110.8, 97.0, 55.7, 54.8, 53.1, 52.3, 32.6, 27.3, 24.4, 15.1; ESI-MS: (*m/z*) 369.0 [M+H]⁺, 390.9 [M+Na]⁺, 366.8 [M-H]⁻; HPLC *method A*: *t_r* = 4.329 min.

(*S*)-3-(3-((7-Chloro-9*H*-pyrimido[4,5-*b*]indol-4-yl)(methyl)amino)piperidin-1-yl)propanenitrile (**(*S*)-5c**)

The title compound was prepared from (*S*)-7-chloro-*N*-methyl-*N*-(piperidin-3-yl)-9*H*-pyrimido[4,5-*b*]indol-4-amine (65.0 mg, 0.21 mmol) and acrylonitrile (21.8 mg, 0.41 mmol) in dry MeOH (20 mL) according to general procedure A. Purification by flash column chromatography (SiO₂, DCM:MeOH gradient elution from 95.5:4.5 to 93.5:6.5) gave 53 mg of a white solid (70% yield); ¹H NMR (200 MHz, DMSO-*d*₆) δ 12.21 (s, 1H), 8.40 (d, *J* = 0.4 Hz, 1H), 7.78 (d, *J* = 8.7 Hz, 1H), 7.47 (d, *J* = 2.0 Hz, 1H), 7.34 (dd, *J* = 8.7, 1.8 Hz, 1H), 4.57 – 4.36 (m, 1H), 3.15 (s, 3H), 3.12 – 3.01 (m, 1H), 2.94 – 2.80 (m, 1H), 2.78 – 2.68 (m, 2H), 2.67 – 2.57 (m, 2H), 2.46 – 2.30 (m, 1H), 2.05 – 1.86 (m, 1H), 1.85 – 1.37 (m, 4H); ¹³C NMR (50 MHz, DMSO-*d*₆) δ 159.4, 157.4, 153.8, 137.3, 129.1, 123.9, 120.6, 120.1, 118.5, 110.8, 97.0,

55.7, 54.8, 53.0, 52.2, 32.6, 27.2, 24.3, 15.0; ESI-MS: (m/z) 369.1 [M+H]⁺, 391.0 [M+Na]⁺, 366.9 [M-H]⁻; HPLC *method A*: t_r = 4.724 min.

3-(3-((7-Bromo-9*H*-pyrimido[4,5-*b*]indol-4-yl)(methyl)amino)piperidin-1-yl)propanenitrile
(5d)

The title compound was prepared from 7-bromo-*N*-methyl-*N*-(piperidin-3-yl)-9*H*-pyrimido[4,5-*b*]indol-4-amine (120.0 mg, 0.33 mmol) and acrylonitrile (26.5 mg, 0.50 mmol) in dry MeOH (10 mL) according to general procedure A. Purification by flash column chromatography (SiO₂, DCM:EtOH gradient elution from 98:2 to 9:1) gave 90 mg (65% yield); ¹H NMR (300 MHz, DMSO-*d*₆) δ 12.20 (s, 1H), 8.40 (s, 1H), 7.73 (d, *J* = 8.7 Hz, 1H), 7.61 (d, *J* = 1.9 Hz, 1H), 7.46 (dd, *J* = 8.6, 1.9 Hz, 1H), 4.51 – 4.39 (m, 1H), 3.14 (s, 3H), 3.10 – 3.03 (m, 1H), 2.90 – 2.81 (m, 1H), 2.76 – 2.67 (m, 2H), 2.67 – 2.58 (m, 2H), 2.44 – 2.33 (m, 1H), 2.01 – 1.88 (m, 1H), 1.80 – 1.64 (m, 3H), 1.58 – 1.41 (m, 1H); ESI-MS: (m/z) 412.9 [M+H]⁺, 434.9 [M+Na]⁺, 410.7 [M-H]⁻; HPLC *method B*: t_r = 5.272 min.

(*R*)-3-(3-((7-Bromo-9*H*-pyrimido[4,5-*b*]indol-4-yl)(methyl)amino)piperidin-1-yl)propanenitrile (**(*R*)-5d**)

The title compound was prepared from (*R*)-7-bromo-*N*-methyl-*N*-(piperidin-3-yl)-9*H*-pyrimido[4,5-*b*]indol-4-amine (65.0 mg, 0.18 mmol) and acrylonitrile (21.1 mg, 0.4 mmol) in HPLC grade MeOH (30 mL) according to general procedure A. Purification by flash column chromatography (SiO₂, DCM:MeOH 95:5) gave 65 mg of a white solid (87% yield); ¹H NMR (300 MHz, DMSO-*d*₆) δ 12.20 (s, 1H), 8.40 (s, 1H), 7.73 (d, *J* = 8.7 Hz, 1H), 7.61 (d, *J* = 1.9 Hz, 1H), 7.46 (dd, *J* = 8.6, 1.9 Hz, 1H), 4.52 – 4.39 (m, 1H), 3.14 (s, 3H), 3.11 – 3.04 (m, 1H), 2.91 – 2.81 (m, 1H), 2.76 – 2.68 (m, 2H), 2.67 – 2.59 (m, 2H), 2.44 – 2.33 (m, 1H), 2.02 – 1.89 (m, 1H), 1.82 – 1.64 (m, 3H), 1.58 – 1.40 (m, 1H); ESI-MS: (m/z) 413.5 [M+H]⁺, 435.5 [M+Na]⁺, 411.5 [M-H]⁻; HPLC *method A*: t_r = 4.038 min.

(*S*)-3-(3-((7-Bromo-9*H*-pyrimido[4,5-*b*]indol-4-yl)(methyl)amino)piperidin-1-yl)propanenitrile (**(*S*)-5d**)

The title compound was prepared from (*S*)-7-bromo-*N*-methyl-*N*-(piperidin-3-yl)-9*H*-pyrimido[4,5-*b*]indol-4-amine (55.0 mg, 0.15 mmol) and acrylonitrile (17.8 mg, 0.34 mmol) in HPLC grade MeOH (25 mL) according to general procedure A. Purification by flash column chromatography (SiO₂, DCM:MeOH 95:5) gave 28 mg of a white solid (44% yield); ¹H NMR (300 MHz, DMSO-*d*₆) δ 12.20 (s, 1H), 8.40 (s, 1H), 7.73 (d, *J* = 8.7 Hz, 1H), 7.61 (d, *J* = 1.9 Hz, 1H), 7.46 (dd, *J* = 8.6, 1.9 Hz, 1H), 4.52 – 4.38 (m, 1H), 3.14 (s, 3H), 3.11 – 3.02 (m, 1H), 2.92 – 2.81 (m, 1H), 2.76 – 2.68 (m, 2H), 2.68 – 2.57 (m, 2H), 2.45 – 2.31 (m, 1H), 2.03 – 1.88 (m, 1H), 1.83 – 1.63 (m, 3H), 1.60 – 1.40 (m, 1H); ESI-MS: (m/z) 413.3 [M+H]⁺, 435.3 [M+Na]⁺, 411.3 [M-H]⁻; HPLC *method A*: t_r = 4.099 min.

3-(3-((7-Methoxy-9*H*-pyrimido[4,5-*b*]indol-4-yl)(methyl)amino)piperidin-1-yl)propanenitrile (**(5e)**)

The title compound was prepared from 7-methoxy-*N*-methyl-*N*-(piperidin-3-yl)-9*H*-pyrimido[4,5-*b*]indol-4-amine (90.0 mg, 0.29 mmol) and acrylonitrile (23.0 mg, 0.43 mmol) in dry MeOH (7 mL) according to general procedure A. Purification by flash column chromatography (SiO₂, DCM:EtOH gradient elution from 98:2 to 9:1) gave 60 mg (57% yield); ¹H NMR (300 MHz, DMSO-*d*₆) δ 11.96 (s, 1H), 8.34 (s, 1H), 7.67 (d, *J* = 8.7 Hz, 1H), 7.01 – 6.89 (m, 1H), 4.52 – 4.35 (m, 1H), 3.83 (s, 3H), 3.11 (s, 3H), 3.06 – 2.98 (m, 1H), 2.90 – 2.81 (m, 1H), 2.76 – 2.57 (m, 4H), 2.43 – 2.32 (m, 1H), 2.00 – 1.87 (m, 1H), 1.83 – 1.63 (m, 3H), 1.59 – 1.40 (m, 1H); ¹³C NMR (101 MHz, DMSO-*d*₆) δ 158.8, 157.6, 157.0, 152.3, 138.0, 123.3, 119.9, 113.1, 109.2, 97.9, 95.1, 55.7, 55.2, 54.5, 53.0, 52.2, 32.2, 27.2, 24.3, 14.9; ESI-MS: (m/z) 365.0 [M+H]⁺, 387.0 [M+Na]⁺, 363.1 [M-H]⁻; HPLC *method B*: t_r = 2.744 min.

3-(3-(Methyl(7-(trifluoromethyl)-9*H*-pyrimido[4,5-*b*]indol-4-yl)amino)piperidin-1-yl)-propanenitrile (**5f**)

The title compound was prepared from *N*-methyl-*N*-(piperidin-3-yl)-7-(trifluoromethyl)-9*H*-pyrimido[4,5-*b*]indol-4-amine (85.0 mg, 0.24 mmol) and acrylonitrile (19.1 mg, 0.36 mmol) in dry MeOH (3 mL) according to general procedure A. Purification twice by flash column chromatography (SiO₂, DCM:EtOH gradient elution from 97:3 to 4:1 and SiO₂, DCM:(2*N* NH₃ in MeOH) gradient elution from 99:1 to 92:8) gave 36 mg (37% yield); ¹H NMR (300 MHz, DMSO-*d*₆) δ 12.44 (s, 1H), 8.44 (s, 1H), 8.00 (d, *J* = 8.5 Hz, 1H), 7.74 (s, 1H), 7.64 (d, *J* = 8.5 Hz, 1H), 4.59 – 4.45 (m, 1H), 3.19 (s, 3H), 3.15 – 3.07 (m, 1H), 2.92 – 2.83 (m, 1H), 2.77 – 2.69 (m, 2H), 2.68 – 2.60 (m, 2H), 2.46 – 2.35 (m, 1H), 2.02 – 1.91 (m, 1H), 1.84 – 1.66 (m, 3H), 1.60 – 1.42 (m, 1H); ESI-MS: (*m/z*) 403.1 [M+H]⁺, 425.0 [M+Na]⁺, 401.0 [M-H]⁻; HPLC *method B*: *t_r* = 5.218 min.

3-(3-((6-Chloro-9*H*-pyrimido[4,5-*b*]indol-4-yl)(methyl)amino)piperidin-1-yl)propanenitrile (**5g**)

The title compound was prepared from 6-chloro-*N*-methyl-*N*-(piperidin-3-yl)-9*H*-pyrimido[4,5-*b*]indol-4-amine (45.0 mg, 0.14 mmol) and acrylonitrile (16.6 mg, 0.31 mmol) in HPLC grade MeOH (13 mL) according to general procedure A. Purification by flash column chromatography (SiO₂, DCM:MeOH gradient elution from 95.5:4.5 to 93.5:6.5) gave 44 mg of a white solid (84% yield); ¹H NMR (400 MHz, DMSO-*d*₆) δ 12.23 (s, 1H), 8.40 (s, 1H), 7.73 (d, *J* = 1.4 Hz, 1H), 7.49 (d, *J* = 8.6 Hz, 1H), 7.41 (dd, *J* = 8.5, 1.5 Hz, 1H), 4.48 – 4.36 (m, 1H), 3.17 (s, 3H), 3.03 – 2.94 (m, 1H), 2.90 – 2.81 (m, 1H), 2.72 – 2.61 (m, 4H), 2.43 – 2.34 (m, 1H), 2.05 – 1.94 (m, 1H), 1.92 – 1.70 (m, 3H), 1.63 – 1.49 (m, 1H); ¹³C NMR (101 MHz, DMSO-*d*₆) δ 159.5, 157.5, 153.9, 135.1, 124.6, 124.4, 121.6, 120.8, 119.8, 112.6, 96.8, 55.4, 54.7, 52.9, 51.9, 32.8, 27.2, 24.3, 14.7; ESI-MS: (*m/z*) 369.4 [M+H]⁺, 391.4 [M+Na]⁺, 367.4 [M-H]⁻; HPLC *method A*: *t_r* = 6.421 min.

3-(3-((6-Bromo-9*H*-pyrimido[4,5-*b*]indol-4-yl)(methyl)amino)piperidin-1-yl)propanenitrile
(5h)

The title compound was prepared from 6-bromo-*N*-methyl-*N*-(piperidin-3-yl)-9*H*-pyrimido[4,5-*b*]indol-4-amine (55.0 mg, 0.15 mmol) and acrylonitrile (17.8 mg, 0.34 mmol) in HPLC grade MeOH (25 mL) according to general procedure A. Purification by flash column chromatography (SiO₂, DCM:MeOH gradient elution from 95.5:4.5 to 93.5:6.5) gave 48 mg of a white solid (76% yield); ¹H NMR (300 MHz, DMSO-*d*₆) δ 12.25 (s, 1H), 8.40 (s, 1H), 7.86 (d, *J* = 1.5 Hz, 1H), 7.53 (dd, *J* = 8.6, 1.7 Hz, 1H), 7.44 (d, *J* = 8.5 Hz, 1H), 4.48 – 4.35 (m, 1H), 3.16 (s, 3H), 3.02 – 2.91 (m, 1H), 2.91 – 2.81 (m, 1H), 2.75 – 2.59 (m, 4H), 2.46 – 2.34 (m, 1H), 2.05 – 1.70 (m, 4H), 1.65 – 1.49 (m, 1H); ¹³C NMR (101 MHz, DMSO-*d*₆) δ 159.5, 157.3, 154.0, 135.4, 127.1, 124.5, 121.4, 119.9, 113.1, 112.5, 96.7, 55.4, 54.8, 52.9, 51.9, 32.7, 27.3, 24.3, 14.7; ESI-MS: (*m/z*) 413.1 [M+H]⁺, 435.0 [M+Na]⁺, 411.1 [M-H]⁻; HPLC *method A*: *t_r* = 4.195 min.

3-(3-((5-Chloro-9*H*-pyrimido[4,5-*b*]indol-4-yl)(methyl)amino)piperidin-1-yl)propanenitrile
(5i)

The title compound was prepared from 5-chloro-*N*-methyl-*N*-(piperidin-3-yl)-9*H*-pyrimido[4,5-*b*]indol-4-amine (47.0 mg, 0.15 mmol) and acrylonitrile (17.4 mg, 0.33 mmol) in HPLC grade MeOH (13.5 mL) according to general procedure A (reaction time 20 h). Purification by flash column chromatography (SiO₂, DCM:MeOH 94.5:5.5) gave 38 mg of a white solid; ¹H NMR (400 MHz, DMSO-*d*₆) δ 12.26 (s, 1H), 8.37 (s, 1H), 7.45 – 7.34 (m, 2H), 7.27 (dd, *J* = 7.5, 0.8 Hz, 1H), 4.49 – 4.33 (m, 1H), 3.03 – 2.76 (m, 5H), 2.71 – 2.54 (m, 4H), 2.37 – 2.19 (m, 1H), 2.01 – 1.46 (m, 5H); ESI-MS: (*m/z*) 369.3 [M+H]⁺, 391.3 [M+Na]⁺, 367.3 [M-H]⁻; HPLC *method A*: *t_r* = 3.343 min.

3-(3-((7-Chloro-2-methyl-9*H*-pyrimido[4,5-*b*]indol-4-yl)(methyl)amino)piperidin-1-yl)propanenitrile (**5j**)

The title compound was prepared from 7-chloro-*N*,2-dimethyl-*N*-(piperidin-3-yl)-9*H*-pyrimido[4,5-*b*]indol-4-amine (60.0 mg, 0.18 mmol) and acrylonitrile (21.2 mg, 0.40 mmol) in HPLC grade MeOH (17 mL) according to general procedure A. Purification by flash column chromatography (SiO₂, DCM:MeOH gradient elution from 96:4 to 94:6) gave 55 mg of a beige solid (79% yield); ¹H NMR (300 MHz, DMSO-*d*₆) δ 11.99 (s, 1H), 7.72 (d, *J* = 8.7 Hz, 1H), 7.44 (d, *J* = 2.0 Hz, 1H), 7.30 (dd, *J* = 8.6, 2.1 Hz, 1H), 4.49 – 4.35 (m, 1H), 3.11 (s, 3H), 3.09 – 3.02 (m, 1H), 2.90 – 2.80 (m, 1H), 2.75 – 2.67 (m, 2H), 2.66 – 2.55 (m, 2H), 2.48 (s, 3H), 2.41 – 2.29 (m, 1H), 2.02 – 1.89 (m, 1H), 1.82 – 1.63 (m, 3H), 1.58 – 1.43 (m, 1H); ¹³C NMR (50 MHz, DMSO-*d*₆) δ 162.6, 159.4, 158.4, 137.4, 128.7, 123.5, 120.5, 120.2, 118.8, 110.8, 94.8, 55.6, 54.8, 53.1, 52.5, 32.4, 27.4, 25.9, 24.4, 15.1; ESI-MS: (*m/z*) 382.9 [M+H]⁺, 404.9 [M+Na]⁺, 380.9 [M-H]⁻; HPLC *method A*: *t_r* = 5.951 min.

Detailed procedures for the preparation of final compound 11

tert-Butyl 3-((7-iodo-9*H*-pyrimido[4,5-*b*]indol-4-yl)(methyl)amino)piperidine-1-carboxylate (**9**)

The title compound was prepared by a two-step procedure. In the first step 4-chloro-7-iodo-9-tosyl-9*H*-pyrimido[4,5-*b*]indole (**6**) (590.0 mg, 1.22 mmol), *N*-Boc-3-(methylamino)piperidine (339.8 mg, 1.59 mmol) and DIPEA (473.0 mg, 3.66 mmol) were stirred in dry DMF (16 mL) at 60°C for 2 h. After cooling down to rt, the mixture was poured into ice-cold and saturated NH₄Cl solution (50 mL) was added. The resulting precipitate was filtered off and dried over P₂O₅ in vacuo to yield 779 mg of crude *tert*-butyl 3-((7-iodo-9-tosyl-9*H*-pyrimido[4,5-*b*]indol-4-yl)(methyl)amino)piperidine-1-carboxylate (**8**) as a beige solid (97% crude yield), used in the

second step without further purification. A small portion was purified by flash column chromatography for analytical purposes (SiO₂, petroleum ether:EtOAc gradient elution from 3:2 to 1:1); ¹H NMR (300 MHz, CDCl₃) δ 8.86 (d, *J* = 1.4 Hz, 1H), 8.62 (s, 1H), 8.09 (d, *J* = 8.4 Hz, 2H), 7.74 (dd, *J* = 8.4, 1.4 Hz, 1H), 7.41 (d, *J* = 7.9 Hz, 1H), 7.27 (d, *J* = 8.1 Hz, 2H; overlap with CHCl₃ signal), 4.47 – 3.90 (m, 3H), 3.11 (s, 3H), 3.08 – 2.98 (m, 1H), 2.77 – 2.60 (m, 1H), 2.37 (s, 3H), 2.01 – 1.71 (m, 3H), 1.64 – 1.29 (m, 10H); ¹³C NMR (50 MHz, CDCl₃) δ 160.5, 157.0, 154.8, 154.4, 145.8, 136.4, 135.4, 133.2, 129.8, 128.2, 124.0, 123.1, 121.3, 101.2, 91.3, 80.0, 55.6 (br), 46.7, 44.1 (br), 33.7 (br), 28.5, 28.1, 24.8, 21.8; ESI-MS: (*m/z*) 684.7 [M+Na]⁺, 660.8 [M-H]⁻; HPLC *method A*: *t_r* = 10.993 min.

Crude *tert*-butyl 3-((7-iodo-9-tosyl-9*H*-pyrimido[4,5-*b*]indol-4-yl)(methyl)amino)piperidine-1-carboxylate (**8**) (680 mg) was dissolved in dry THF (30 mL). *Kt*BuO (807.4 mg, 7.2 mmol) was added and the mixture stirred at rt for 1 h. Saturated NH₄Cl solution (50 mL) was added and the mixture was extracted with EtOAc (3 x 30 mL). Combined organic layers were dried over Na₂SO₄ and concentrated under reduced pressure. Purification of the residue twice by flash column chromatography (SiO₂, DCM:MeOH 95:5 and SiO₂, DCM:MeOH gradient elution from 97.5:2.5 to 93:7) gave 292 mg of a beige solid (56% yield); ¹H NMR (300 MHz, CDCl₃) δ 11.30 (s, 1H), 8.52 (s, 1H), 7.92 (d, *J* = 1.1 Hz, 1H), 7.61 (dd, *J* = 8.5, 1.4 Hz, 1H), 7.53 (d, *J* = 8.5 Hz, 1H), 4.55 – 4.04 (m, 3H), 3.29 (s, 3H), 3.11 – 2.98 (m, 1H), 2.78 – 2.61 (m, 1H), 2.10 – 1.76 (m, 3H), 1.74 – 1.30 (m, 10H); ESI-MS: (*m/z*) 530.6 [M+Na]⁺, 506.6 [M-H]⁻; HPLC *method A*: *t_r* = 9.541 min.

7-Iodo-*N*-methyl-*N*-(piperidin-3-yl)-9*H*-pyrimido[4,5-*b*]indol-4-amine (**10**)

tert-Butyl 3-((7-iodo-9*H*-pyrimido[4,5-*b*]indol-4-yl)(methyl)amino)piperidine-1-carboxylate (**9**) (240.0 mg, 0.473 mmol) was suspended in dry DCM (7 mL) and TFA was added (1.5 mL). The mixture was stirred at rt for 30 min and then concentrated under reduced pressure. Residual TFA was neutralised by addition of saturated NaHCO₃ solution (30 mL) which resulted in a

precipitate. The precipitate was filtered off, washed with saturated NaHCO₃ solution and demineralised water and dried over P₂O₅ *in vacuo*. 199 mg of a beige solid were yielded (>100% crude yield) and used in the next step without further purification; ¹H NMR (300 MHz, MeOD) δ 8.35 (s, 1H), 7.86 (s, 1H), 7.65 – 7.52 (m, 2H), 4.55 – 4.40 (m, 1H), 3.24 (s, 3H), 3.14 – 3.05 (m, 1H), 3.02 – 2.84 (m, 2H), 2.60 – 2.47 (m, 1H), 2.15 – 1.84 (m, 3H), 1.77 – 1.59 (m, 1H); ESI-MS: (m/z) 408.3 [M+H]⁺, 406.3 [M-H]⁻; HPLC *method A*: t_r = 4.563 min.

3-(3-((7-Iodo-9*H*-pyrimido[4,5-*b*]indol-4-yl)(methyl)amino)piperidin-1-yl)propanenitrile (**11**)

The title compound was prepared from 7-Iodo-*N*-methyl-*N*-(piperidin-3-yl)-9*H*-pyrimido[4,5-*b*]indol-4-amine (**10**) (70.0 mg, 0.17 mmol) and acrylonitrile (20.1 mg, 0.38 mmol) in HPLC grade MeOH (30 mL) according to general procedure A. Purification by flash column chromatography (SiO₂, DCM:MeOH 95:5) gave 35 mg of a white solid (44% yield); ¹H NMR (400 MHz, DMSO-*d*₆) δ 12.15 (s, 1H), 8.40 (s, 1H), 7.79 (s, 1H), 7.67 – 7.53 (m, 2H), 4.51 – 4.37 (m, 1H), 3.13 (s, 3H), 3.09 – 3.01 (m, 1H), 2.90 – 2.80 (m, 1H), 2.76 – 2.67 (m, 2H), 2.67 – 2.58 (m, 2H), 2.42 – 2.31 (m, 1H), 2.01 – 1.89 (m, 1H), 1.82 – 1.63 (m, 3H), 1.58 – 1.41 (m, 1H); ¹³C NMR (101 MHz, DMSO-*d*₆) δ 159.5, 156.9, 153.9, 137.9, 128.9, 124.4, 120.0, 119.5, 119.2, 97.1, 89.3, 55.6, 54.7, 53.0, 52.2, 32.5, 27.2, 24.3, 15.0; ESI-MS: (m/z) 461.2 [M+H]⁺, 483.2 [M+Na]⁺, 459.2 [M-H]⁻; HPLC *method A*: t_r = 5.555 min.

Detailed procedures for the preparation of final compound **15**

tert-Butyl 3-(methyl(7-((trimethylsilyl)ethynyl)-9*H*-pyrimido[4,5-*b*]indol-4-yl)amino)piperidine-1-carboxylate (**12**)

A mixture of *tert*-butyl 3-((7-iodo-9*H*-pyrimido[4,5-*b*]indol-4-yl)(methyl)amino)piperidine-1-carboxylate (**9**) (310.0 mg, 0.61 mmol), CuI (23.3 mg, 0.12 mmol) and Pd(PPh₃)₄ (70.6 mg, 0.06 mmol) in dry DMF was degassed under reduced pressure by sonication and subsequently

set under Ar atmosphere. TMS-acetylene (180.0 mg, 1.83 mmol) and TEA (123.0 mg, 1.22 mmol) were added and the mixture stirred at 50°C and under Ar atmosphere overnight. After cooling down to rt, saturated NH₄Cl solution (3 mL) was added and the mixture was extracted with EtOAc (5 x 3 mL). Combined organic layers were washed with saturated NaCl solution (4 x 7 mL), dried over Na₂SO₄ and concentrated under reduced pressure. Purification of the residue by flash column chromatography (SiO₂, DCM:MeOH gradient elution from 30:1 to 93:7) gave 280 mg of a brown solid (96% yield) containing approx. 10% of an impurity, which was detected in the ¹H NMR and is assumed to be triphenylphosphine oxide; ¹H NMR (400 MHz, CDCl₃) δ 11.81 (s, 1H), 8.61 (s, 1H), 7.72 (d, *J* = 8.3 Hz, 1H), 7.64 (s, 1H), 7.39 (dd, *J* = 8.3, 1.4 Hz, 1H), 4.55 – 4.02 (m, 3H), 3.28 (s, 3H), 3.11 – 3.00 (m, 1H), 2.75 – 2.60 (m, 1H), 2.11 – 2.04 (m, 1H), 1.97 – 1.77 (m, 2H), 1.70 – 1.57 (m, 1H), 1.42 (s, 9H), 0.29 (s, 9H); ESI-MS: (*m/z*) 500.4 [M+Na]⁺, 476.5 [M-H]⁻; HPLC *method A*: *t_r* = 11.448 min.

N-Methyl-*N*-(piperidin-3-yl)-7-((trimethylsilyl)ethynyl)-9*H*-pyrimido[4,5-*b*]indol-4-amine
(13)

tert-Butyl 3-(methyl(7-((trimethylsilyl)ethynyl)-9*H*-pyrimido[4,5-*b*]indol-4-yl)amino)piperidine-1-carboxylate (12) (115.2 mg, 0.24 mmol) was suspended in dry 4*N* HCl in 1,4-dioxane (6 mL). The mixture was stirred at rt for 20 min (the reaction time was strictly kept short to prevent by-product formation). Saturated NaHCO₃ solution (20 mL) was added for neutralisation and the mixture extracted with EtOAc (10 x 20 mL). Combined organic layers were dried over Na₂SO₄ and concentrated under reduced pressure. Purification of the residue by flash column chromatography (SiO₂, DCM:(2*N* NH₃ in MeOH) 9:1) gave 38 mg of a solid (42% yield); ¹H NMR (400 MHz, MeOD) δ 8.33 (s, 1H), 7.76 (d, *J* = 8.4 Hz, 1H), 7.56 (s, 1H), 7.35 (d, *J* = 8.3 Hz, 1H), 4.54 – 4.45 (m, 1H), 3.26 (s, 3H), 3.13 – 3.07 (m, 1H), 3.02 – 2.95 (m, 1H), 2.94 – 2.86 (m, 1H), 2.59 – 2.49 (m, 1H), 2.14 – 1.87 (m, 3H), 1.76 – 1.63 (m, 1H), 0.26 (s, 9H); HPLC *method A*: *t_r* = 7.008 min.

3-(3-((7-Ethynyl-9*H*-pyrimido[4,5-*b*]indol-4-yl)(methyl)amino)piperidin-1-yl)propanenitrile
(15)

Acrylonitrile (8.0 mg, 0.15 mmol) and TEA (15.3 mg, 0.15 mmol) were added to a stirring solution of *N*-methyl-*N*-(piperidin-3-yl)-7-((trimethylsilyl)ethynyl)-9*H*-pyrimido[4,5-*b*]indol-4-amine (13) in HPLC grade MeOH (20 mL) and the mixture was stirred at rt and under N₂ atmosphere. Due to slow conversion, reactants were added repeatedly: acrylonitrile (8.0 mg, 0.15 mmol) and TEA (15.3 mg, 0.15 mmol) after 3 h of stirring and additional acrylonitrile (4.0 mg, 0.08 mmol) and TEA (7.7 mg, 0.08 mmol) after 6 h of stirring. After stirring at rt and under N₂ atmosphere overnight, K₂CO₃ (16.7 mg, 0.12 mmol) was added to initiate the TMS deprotection and stirring continued. Additional K₂CO₃ (10.0 mg, 0.07 mmol) was added and stirring continued for 2 days. The mixture was concentrated under reduced pressure and the residue was purified three times by flash column chromatography (1.SiO₂, DCM:MeOH 95:5, 2.SiO₂, DCM:(2N NH₃ in MeOH) gradient elution from 96.5:3.5 to 93:7 and 3.SiO₂, DCM:MeOH gradient elution from 96.5:3.5 to 93:7) to yield 15 mg of a light beige solid (41% yield); ¹H NMR (400 MHz, DMSO-*d*₆) δ 12.18 (s, 1H), 8.39 (s, 1H), 7.79 (d, *J* = 8.4 Hz, 1H), 7.54 (d, *J* = 1.1 Hz, 1H), 7.40 (dd, *J* = 8.3, 1.4 Hz, 1H), 4.56 – 4.41 (m, 1H), 4.19 (s, 1H), 3.16 (s, 3H), 3.13 – 3.06 (m, 1H), 2.94 – 2.84 (m, 1H), 2.80 – 2.59 (m, 4H), 2.47 – 2.35 (m, 1H), 2.06 – 1.90 (m, 1H), 1.89 – 1.67 (m, 3H), 1.60 – 1.45 (m, 1H); ¹³C NMR (101 MHz, DMSO-*d*₆) δ 159.5, 157.6, 153.9, 136.2, 124.0, 122.7, 120.1, 117.4, 114.3, 97.2, 84.2, 80.4, 55.6, 54.6, 53.0, 52.2, 32.7, 27.1, 24.2, 14.9; ESI-MS: (*m/z*) 359.1 [M+H]⁺, 381.1 [M+Na]⁺, 357.0 [M-H]⁻; HPLC method A: *t*_r = 3.865 min.

Detailed procedures for the preparation of final compound (S)-15

tert-Butyl (*S*)-3-((7-iodo-9-tosyl-9*H*-pyrimido[4,5-*b*]indol-4-yl)amino)piperidine-1-carboxylate ((*S*)-7)

4-Chloro-7-iodo-9-tosyl-9*H*-pyrimido[4,5-*b*]indole (**6**) (500.0 mg, 1.03 mmol), (*S*)-*N*-Boc-3-aminopiperidine (288.8 mg, 1.45 mmol) and DIPEA (399.3 mg, 3.09 mmol) were stirred in dry DMF (14 mL) at 80°C for 16 h. After cooling down to rt, the mixture was poured into ice-cold water and saturated NH₄Cl solution (75 mL) was added. The mixture was extracted twice with EtOAc (175 mL and 25 mL). Combined organic layers were washed with saturated NaCl solution (3 x 30 mL), dried over Na₂SO₄ and concentrated under reduced pressure. Purification of the residue by flash column chromatography (SiO₂, petroleum ether:(EtOAc+MeOH 95+5) 2:1) gave 360 mg of a yellow solid (54% yield); ESI-MS: 671.0 [M+Na]⁺, 646.9 [M-H]⁻; HPLC *method A*: t_r = 11.182 min.

tert-Butyl (*S*)-3-((7-iodo-9*H*-pyrimido[4,5-*b*]indol-4-yl)(methyl)amino)piperidine-1-carboxylate ((*S*)-9)

The title compound was prepared by a two-step procedure. In the first step a solution of *tert*-butyl (*S*)-3-((7-iodo-9-tosyl-9*H*-pyrimido[4,5-*b*]indol-4-yl)amino)piperidine-1-carboxylate ((*S*)-7) (342.0 mg, 0.53 mmol) in dry DMF (6 mL) was stirred in a flame-dried Schlenk tube under Ar atmosphere and cooled to 0 °C. NaH (31.0 mg of a 60% dispersion in mineral oil, 0.752 mmol) was added and the mixture stirred for 30 minutes for deprotonation. The mixture was then cooled by an MeOH/ice bath before iodomethane (112.5 mg, 0.79 mmol) was added. Stirring was continued under Ar atmosphere for 2.5 h leaving the mixture to warm to rt. Saturated NH₄Cl solution (5 mL) was added and the mixture poured into ice-cold water, which was then extracted with EtOAc (3 x 50 mL). Combined organic layers were dried over Na₂SO₄ and concentrated under reduced pressure to afford 368 mg of crude (*S*)-3-((7-iodo-9-tosyl-9*H*-pyrimido[4,5-*b*]indol-4-yl)(methyl)amino)piperidine-1-carboxylate ((*S*)-8), which was used in the second step without further purification. The crude material was dissolved in dry THF (15

mL). K_tBuO (414.7 mg, 3.70 mmol) was added and the mixture stirred at rt for 2.5 h. Saturated NH₄Cl solution (20 mL) was added and the mixture extracted with EtOAc (3 x 20 mL). Combined organic layers were dried over Na₂SO₄ and concentrated under reduced pressure. Purification of the residue by flash column chromatography (SiO₂, DCM:MeOH gradient elution from 97.5:2.5 to 96.5:3.5) gave 157 mg of a white solid (59% yield); ¹H NMR (400 MHz, CDCl₃) δ 11.58 (br s, 1H), 8.55 (s, 1H), 7.89 (s, 1H), 7.59 (dd, *J* = 8.5, 1.3 Hz, 1H), 7.53 (d, *J* = 8.5 Hz, 1H), 4.52 – 4.00 (m, 3H), 3.27 (s, 3H), 3.10 – 3.00 (m, 1H), 2.76 – 2.60 (m, 1H), 2.10 – 1.77 (m, 3H), 1.71 – 1.56 (m, 1H), 1.43 (s, 9H).; ESI-MS: 508.9 [M+H]⁺, 530.9 [M+Na]⁺, 506.9 [M-H]⁻; HPLC *method A*: t_r = 10.246 min.

(*S*)-7-Iodo-*N*-methyl-*N*-(piperidin-3-yl)-9*H*-pyrimido[4,5-*b*]indol-4-amine ((*S*)-**10**)

tert-Butyl (*S*)-3-((7-iodo-9*H*-pyrimido[4,5-*b*]indol-4-yl)(methylamino)piperidine-1-carboxylate ((*S*)-**9**) (140.0 mg, 0.28 mmol) was stirred in a mixture of dry DCM (4 mL) and TFA (0.8 mL) at rt for 1 h. The mixture was concentrated under reduced pressure and residual TFA was neutralized by addition of saturated NaHCO₃ solution (30 mL). The mixture was then extracted with EtOAc (3 x 25 mL), adding MeOH to improve the solubility of the product in the organic layer. Combined organic layers were washed with saturated NaHCO₃ solution (3 x 30 mL), dried over Na₂SO₄ and evaporated to dryness to afford 113 mg of a beige solid (100% yield); ¹H NMR (400 MHz, MeOD) δ 8.35 (s, 1H), 7.85 (s, 1H), 7.61 – 7.54 (m, 2H), 4.53 – 4.44 (m, 1H), 3.24 (s, 3H), 3.15 – 3.08 (m, 1H), 3.03 – 2.96 (m, 1H), 2.95 – 2.87 (m, 1H), 2.61 – 2.50 (m, 1H), 2.13 – 1.86 (m, 3H), 1.76 – 1.63 (m, 1H); ESI-MS: (*m/z*) 408.5 [M+H]⁺, 406.5 [M-H]⁻; HPLC *method A*: t_r = 5.134 min.

(*S*)-3-(3-((7-Iodo-9*H*-pyrimido[4,5-*b*]indol-4-yl)(methylamino)piperidin-1-yl)propanenitrile ((*S*)-**11**)

Acrylonitrile (16.6 mg, 0.31 mmol) and triethylamine (26.5 mg, 0.26 mmol) were added to a stirring solution of (*S*)-7-iodo-*N*-methyl-*N*-(piperidin-3-yl)-9*H*-pyrimido[4,5-*b*]indol-4-amine ((**S**)-**10**) (107.0 mg, 0.26 mmol) in HPLC grade MeOH (45 mL). The mixture was stirred at rt for 16 h and then concentrated under reduced pressure. Purification of the residue by flash column chromatography (SiO₂, DCM:MeOH gradient elution from 95:5 to 92.5:7.5) gave 89 mg of a white solid (74% yield); ¹H NMR (400 MHz, DMSO-*d*₆) δ 12.15 (s, 1H), 8.40 (s, 1H), 7.79 (d, *J* = 1.2 Hz, 1H), 7.62 (dd, *J* = 8.5, 1.5 Hz, 1H), 7.58 (d, *J* = 8.5 Hz, 1H), 4.51 – 4.38 (m, 1H), 3.13 (s, 3H), 3.09 – 3.02 (m, 1H), 2.89 – 2.81 (m, 1H), 2.75 – 2.67 (m, 2H), 2.67 – 2.58 (m, 2H), 2.41 – 2.32 (m, 1H), 2.00 – 1.88 (m, 1H), 1.81 – 1.65 (m, 3H), 1.56 – 1.42 (m, 1H); ¹³C NMR (101 MHz, DMSO-*d*₆) δ 159.5, 156.9, 154.0, 137.9, 129.0, 124.4, 120.1, 119.6, 119.2, 97.1, 89.4, 55.7, 54.8, 53.0, 52.2, 32.6, 27.3, 24.3, 15.0.

(*S*)-3-(3-(Methyl(7-((trimethylsilyl)ethynyl)-9*H*-pyrimido[4,5-*b*]indol-4-yl)amino)piperidin-1-yl)propanenitrile ((**S**)-**14**)

A solution of (*S*)-3-(3-((7-iodo-9*H*-pyrimido[4,5-*b*]indol-4-yl)(methyl)amino)piperidin-1-yl)propanenitrile ((**S**)-**11**) (40.0 mg, 0.09 mmol) and CuI (1.65 mg, 0.009 mmol) in dry DMF (1.5 mL) was degassed and stirred in a Schlenk tube under Ar atmosphere. Triethylamine (17.6 mg, 0.17 mmol) and trimethylsilylacetylen (25.6 mg, 0.26 mmol) were added under Ar flow, followed by a small amount of bis(triphenylphosphine)palladium(II) dichloride (5 mg, 0.007 mmol). The mixture was stirred at rt for 2 h, then diluted with EtOAc and washed with saturated NaHCO₃ solution (2 x 10 mL). The organic layer was dried over Na₂SO₄ and concentrated under reduced pressure. Purification of the residue by flash column chromatography (SiO₂, DCM:MeOH 95:5) gave 32 mg of a yellow solid (86% yield); ¹H NMR (400 MHz, CDCl₃) δ 12.49 (br s, 1H), 8.59 (br s, 1H), 7.69 (d, *J* = 8.4 Hz, 1H), 7.63 (s, 1H), 7.40 (dd, *J* = 8.3, 0.8 Hz, 1H), 4.71 – 4.58 (m, 1H), 3.27 (s, 3H), 3.19 – 3.12 (m, 1H), 2.98 – 2.91 (m, 1H), 2.85 – 2.74 (m, 2H), 2.58 (t, *J* = 7.0 Hz, 2H), 2.50 – 2.41 (m, 1H), 2.15 – 2.07 (m, 1H), 2.03 – 1.94 (m,

1H), 1.90 – 1.71 (m, 3H), 0.35 – 0.21 (m, 9H); ¹³C NMR (101 MHz, CDCl₃) δ 160.2, 157.8, 153.0, 136.4, 124.9, 122.6, 120.5, 119.5, 118.8, 115.0, 105.8, 98.8, 94.5, 56.1, 55.1, 53.8, 53.1, 33.6, 27.9, 24.6, 16.0, 0.2; ESI-MS: (m/z) 431.7 [M+H]⁺, 453.7 [M+Na]⁺, 429.7 [M-H]⁻; HPLC *method A*: t_r = 7.262 min.

(*S*)-3-(3-((7-Ethynyl-9*H*-pyrimido[4,5-*b*]indol-4-yl)(methyl)amino)piperidin-1-yl)propanenitrile ((*S*)-**15**)

(*S*)-3-(3-(methyl(7-((trimethylsilyl)ethynyl)-9*H*-pyrimido[4,5-*b*]indol-4-yl)amino)piperidin-1-yl)propanenitrile ((*S*)-**14**) (32.0 mg, 0.07 mmol) and K₂CO₃ (12.0 mg, 0.09 mmol) were stirred in HPLC grade MeOH (4 mL) at rt and under N₂ atmosphere for 3 h. The mixture was concentrated under reduced pressure and the residue redissolved in EtOAc. The solution was washed with saturated NaHCO₃ solution (2 x 15 mL), dried over Na₂SO₄ and concentrated under reduced pressure. Purification of the residue by flash column chromatography (SiO₂, DCM:MeOH 95:5) gave 18 mg of a white solid (68% yield); ¹H NMR (400 MHz, DMSO-*d*₆) δ 12.18 (s, 1H), 8.39 (s, 1H), 7.79 (d, *J* = 8.4 Hz, 1H), 7.54 (s, 1H), 7.40 (dd, *J* = 8.3, 1.1 Hz, 1H), 4.53 – 4.43 (m, 1H), 4.19 (s, 1H), 3.16 (s, 3H), 3.11 – 3.04 (m, 1H), 2.90 – 2.83 (m, 1H), 2.76 – 2.68 (m, 2H), 2.67 – 2.58 (m, 2H), 2.43 – 2.33 (m, 1H), 2.01 – 1.90 (m, 1H), 1.83 – 1.66 (m, 3H), 1.60 – 1.43 (m, 1H); ¹³C NMR (101 MHz, DMSO-*d*₆) δ 159.5, 157.6, 153.8, 136.2, 124.0, 122.6, 120.0, 119.9, 117.3, 114.2, 97.2, 84.1, 80.2, 55.6, 54.7, 53.0, 52.2, 32.6, 27.2, 24.3, 15.0; ESI-MS: (m/z) 359.9 [M+H]⁺, 381.9 [M+Na]⁺, 357.8 [M-H]⁻; HPLC *method A*: t_r = 3.237 min.

Detailed procedures for the preparation of final compounds 5k-m

3-(3-(Methyl(7-phenyl-9*H*-pyrimido[4,5-*b*]indol-4-yl)amino)piperidin-1-yl)propanenitrile (**5k**)

Degassed dry dioxane (4 mL) and degassed 0.5M aq. K₃PO₄ solution (1 mL) were added to 3-((7-chloro-9*H*-pyrimido[4,5-*b*]indol-4-yl)(methylamino)piperidin-1-yl)propanenitrile (**1**) (60.0 mg, 0.16 mmol), phenylboronic acid (31.7 mg, 0.26 mmol) and XPhos Pd G3 (4.1 mg, 0.005 mmol) under Ar atmosphere. The mixture was stirred at 100°C for 3 h. After cooling down to rt, saturated NaCl solution (3 mL) was added and the mixture extracted with EtOAc (5 x 3 mL). DCM and MeOH were added to improve the solubility of the product in the organic layer. Combined organic layers washed with saturated NaHCO₃ solution (3 x 20 mL), dried over Na₂SO₄ and concentrated under reduced pressure. Purification of the residue by flash column chromatography (SiO₂, DCM:MeOH gradient elution from 95:5 to 92.5:7.5) gave 40 mg of an off-white solid (60% yield); ¹H NMR (300 MHz, DMSO-*d*₆) δ 12.18 (s, 1H), 8.40 (s, 1H), 7.88 (d, *J* = 8.5 Hz, 1H), 7.78 – 7.68 (m, 3H), 7.64 (dd, *J* = 8.4, 1.5 Hz, 1H), 7.54 – 7.45 (m, 2H), 7.42 – 7.34 (m, 1H), 4.60 – 4.46 (m, 1H), 3.17 (s, 3H), 3.13 – 3.05 (m, 1H), 2.93 – 2.83 (m, 1H), 2.77 – 2.58 (m, 4H), 2.46 – 2.34 (m, 1H), 2.03 – 1.89 (m, 1H), 1.86 – 1.66 (m, 3H), 1.63 – 1.42 (m, 1H); ¹³C NMR (101 MHz, DMSO-*d*₆) δ 159.4, 157.4, 153.4, 140.4, 137.3, 136.8, 129.0, 127.2, 126.7, 122.9, 120.0, 119.6, 118.9, 108.9, 97.4, 55.7, 54.7, 53.0, 52.2, 32.5, 27.3, 24.3, 15.0; ESI-MS: (*m/z*) 411.1 [M+H]⁺, 433.1 [M+Na]⁺, 409.2 [M-H]⁻; HPLC *method A*: *t_r* = 5.034 min.

3-(3-((7-(Furan-2-yl)-9*H*-pyrimido[4,5-*b*]indol-4-yl)(methylamino)piperidin-1-yl)propanenitrile (**5l**)

Degassed dry dioxane (4 mL) and degassed 0.5M aq. K₃PO₄ solution (1 mL) were added to 3-((7-chloro-9*H*-pyrimido[4,5-*b*]indol-4-yl)(methylamino)piperidin-1-yl)propanenitrile (**1**) (60.0 mg, 0.16 mmol), 2-furanylboronic acid (29.1 mg, 0.26 mmol) and XPhos Pd G3 (4.1 mg, 0.005 mmol) in a reaction tube. The tube was sealed and the mixture stirred at 100°C for 3 h. After cooling down to rt, saturated NaCl solution (3 mL) was added and the mixture extracted with EtOAc (5 x 3 mL). DCM and MeOH were added to improve the solubility of the product

in the organic layer. Combined organic layers washed with saturated NaHCO₃ solution. The combined NaHCO₃ solution layers were extracted once more with DCM. The organic layers were unified, dried over Na₂SO₄ and concentrated under reduced pressure. Purification of the residue by flash column chromatography (SiO₂, DCM:MeOH gradient elution from 96:4 to 93:7) gave 43 mg of a beige solid (66% yield); ¹H NMR (400 MHz, DMSO-*d*₆) δ 12.17 (s, 1H), 8.39 (s, 1H), 7.82 (d, *J* = 8.5 Hz, 1H), 7.79 – 7.72 (m, 2H), 7.68 (dd, *J* = 8.4, 1.1 Hz, 1H), 6.96 (d, *J* = 3.2 Hz, 1H), 6.62 (dd, *J* = 3.2, 1.7 Hz, 1H), 4.56 – 4.43 (m, 1H), 3.16 (s, 3H), 3.11 – 3.02 (m, 1H), 2.92 – 2.82 (m, 1H), 2.78 – 2.58 (m, 4H), 2.45 – 2.34 (m, 1H), 2.03 – 1.90 (m, 1H), 1.86 – 1.68 (m, 3H), 1.60 – 1.45 (m, 1H); ¹³C NMR (101 MHz, DMSO-*d*₆) δ 159.3, 157.5, 153.5, 153.4, 142.8, 137.0, 126.9, 122.9, 120.0, 118.8, 116.7, 112.1, 105.6, 105.5, 97.5, 55.6, 54.7, 53.0, 52.1, 32.5, 27.2, 24.3, 14.9; ESI-MS: (*m/z*) 401.1 [M+H]⁺, 423.1 [M+Na]⁺, 399.1 [M-H]⁻; HPLC *method A*: *t*_r = 4.069 min.

4-((1-(2-Cyanoethyl)piperidin-3-yl)(methyl)amino)-9*H*-pyrimido[4,5-*b*]indole-7-carbonitrile
(**5m**)

Degassed dry 1,4-dioxane (2 mL) and degassed 0.01M aq. KOAc solution (2 mL) were added to 3-(3-((7-chloro-9*H*-pyrimido[4,5-*b*]indol-4-yl)(methyl)amino)piperidin-1-yl)propanenitrile (**1**) (60.0 mg, 0.16 mmol), K₄[Fe(CN)₆]·3H₂O (41.2 mg, 0.10 mmol), BrettPhos Pd G3 (5.2 mg, 0.006 mmol) and BrettPhos (3.1 mg, 0.006 mmol) under Ar atmosphere. The mixture was stirred at 100°C and under Ar atmosphere for 2.5 h. Additional BrettPhos Pd G3 and BrettPhos catalysts were added (1.0 mg each) to promote conversion and stirring continued at 10 0°C for 2 h, but the conversion seized at ~85%. After cooling down to rt, saturated NaCl solution (3 mL) was added and the mixture extracted with EtOAc (6 x 3 mL). Combined organic layers were dried over Na₂SO₄ and concentrated under reduced pressure. Purification of the residue twice by flash column chromatography (1.SiO₂, petroleum ether:(EtOAc+MeOH 95+5) gradient elution from 1:1 to 0:1 and 2.SiO₂, DCM:MeOH gradient elution from 95.5:4.5 to

93.5:6.5) gave 15 mg of an off-white solid (26% yield); ^1H NMR (400 MHz, $\text{DMSO-}d_6$) δ 12.50 (s, 1H), 8.44 (s, 1H), 7.95 (d, $J = 8.4$ Hz, 1H), 7.88 (s, 1H), 7.67 (dd, $J = 8.4, 1.2$ Hz, 1H), 4.58 – 4.41 (m, 1H), 3.19 (s, 3H), 3.14 – 3.06 (m, 1H), 2.96 – 2.82 (m, 1H), 2.79 – 2.56 (m, 4H), 2.47 – 2.31 (m, 1H), 2.06 – 1.89 (m, 1H), 1.87 – 1.65 (m, 3H), 1.61 – 1.47 (m, 1H); ^{13}C NMR (101 MHz, $\text{DMSO-}d_6$) δ 159.8, 158.2, 154.7, 135.8, 123.5, 123.4, 123.3, 119.6, 114.9, 105.9, 96.8, 55.4, 54.8, 52.9, 52.1, 32.9, 27.0, 24.2, 15.0; ESI-MS: (m/z) 360.1 $[\text{M}+\text{H}]^+$, 382.1 $[\text{M}+\text{Na}]^+$, 358.1 $[\text{M}-\text{H}]^-$; HPLC *method A*: $t_r = 3.062$ min.

Detailed procedures for the preparation of intermediates 16-18

3-(1-(7-Fluoro-9-tosyl-9H-pyrimido[4,5-*b*]indol-4-yl)octahydro-6H-pyrrolo[2,3-*c*]pyridin-6-yl)propanenitrile (**16**)

4-Chloro-7-fluoro-9-tosyl-9H-pyrimido[4,5-*b*]indole (**3b**) (200.0 mg, 0.53 mmol), 3-(octahydro-6H-pyrrolo[2,3-*c*]pyridin-6-yl)propanenitrile (used as TFA salt and calculated to 37.2 mg of the free base, 0.21 mmol,) and DIPEA (275.3 mg, 2.13 mmol) were stirred in dry DMF (6 mL) at 70 °C for 2.5 h. Additional 3-(octahydro-6H-pyrrolo[2,3-*c*]pyridin-6-yl)propanenitrile (used as TFA salt and calculated to 71.0 mg of the free base, 0.40 mmol) and DIPEA (137.7 mg, 1.07 mmol) were added and stirring at 70 °C continued for 5 h. After cooling down to rt, saturated NaCl solution (15 mL) was added and the mixture extracted with EtOAc (3 x 25 mL). Combined organic layers were washed with saturated NaCl solution (3 x 25 mL), dried over Na_2SO_4 and concentrated under reduced pressure. Purification of the residue by flash column chromatography (SiO_2 , petroleum ether:(EtOAc+MeOH 95+5) gradient elution from 2:1 to 1:3) gave 113 mg of a solid (41% yield); ^1H NMR (400 MHz, CDCl_3) δ 8.51 (s, 1H), 8.22 (d, $J = 9.8$ Hz, 1H), 8.10 (d, $J = 8.4$ Hz, 2H), 7.82 (br s, 1H), 7.26 (d, $J = 8.2$ Hz, 2H, overlap with CHCl_3 signal), 7.14 (td, $J = 8.7, 2.0$ Hz, 1H), 4.67 – 4.50 (m, 1H), 4.28 – 4.08 (m, 1H), 3.50 – 3.41 (m, 1H), 3.19 – 2.98 (m, 1H), 2.91 – 2.53 (m, 4H), 2.52 – 2.13 (m, 7H), 1.99

– 1.81 (m, 3H), 1.69 – 1.56 (m, 1H); ESI-MS: (m/z) 519.5 [M+H]⁺, 541.5 [M+Na]⁺, 517.6 [M-H]⁻; HPLC *method A*: t_r = 6.594 min.

3-(1-(7-Bromo-9-tosyl-9*H*-pyrimido[4,5-*b*]indol-4-yl)octahydro-6*H*-pyrrolo[2,3-*c*]pyridin-6-yl)propanenitrile (**17**)

7-Bromo-4-chloro-9-tosyl-9*H*-pyrimido[4,5-*b*]indole (**3d**) (92.0 mg, 0.21 mmol), 3-(octahydro-6*H*-pyrrolo[2,3-*c*]pyridin-6-yl)propanenitrile (41.5 mg of the free base, 0.23 mmol) and DIPEA (81.7 mg, 0.63 mmol) were stirred in dry DMF (2.5 mL) at 75 °C for 1.5 h. Additional 3-(octahydro-6*H*-pyrrolo[2,3-*c*]pyridin-6-yl)propanenitrile (10.0 mg of the free base, 0.06 mmol) was added and stirring at 75 °C continued for 3 h. Saturated NaCl solution (10 mL) was added and the mixture extracted with EtOAc (3 x 20 mL). Combined organic layers were washed with saturated NaCl solution (3 x 20 mL), dried over Na₂SO₄ and concentrated under reduced pressure. Purification of the residue by flash column chromatography (SiO₂, petroleum ether:(EtOAc + MeOH 95+5) gradient elution from 2:1 to 1:3) gave 66 mg of an off-white solid (54% yield); ESI-MS: 579.7 [M+H]⁺, 601.7 [M+Na]⁺; HPLC *method A*: t_r = 7.363 min.

3-(1-(7-Iodo-9-tosyl-9*H*-pyrimido[4,5-*b*]indol-4-yl)octahydro-6*H*-pyrrolo[2,3-*c*]pyridin-6-yl)propanenitrile (**18**)

4-Chloro-7-iodo-9-tosyl-9*H*-pyrimido[4,5-*b*]indole (**6**) (200.0 mg, 0.41 mmol), 3-(octahydro-6*H*-pyrrolo[2,3-*c*]pyridin-6-yl)propanenitrile (used as TFA salt and calculated to 83.8 mg of the free base, 0.47 mmol) and DIPEA (213.7 mg, 1.65 mmol) were stirred in dry DMF (6 mL) at 75 °C for 2.5 h. After cooling down to rt, saturated NaCl solution (15 mL) was added and the mixture extracted with EtOAc (3 x 25 mL). Combined organic layers were washed with saturated NaCl solution (3 x 20 mL), dried over Na₂SO₄ and concentrated under reduced pressure. Purification of the residue by flash column chromatography (SiO₂, petroleum

ether:(EtOAc+MeOH 95+5) gradient elution from 2:1 to 1:3) gave 158 mg of a solid (61% yield); ¹H NMR (400 MHz, CDCl₃) δ 8.84 (s, 1H), 8.53 (s, 1H), 8.09 (d, *J* = 8.4 Hz, 2H), 7.69 (d, 1H), 7.66 – 7.51 (br s, 1H), 7.27 (d, *J* = 7.3 Hz, 2H, overlap with CHCl₃ signal), 4.62 – 4.45 (m, 1H), 4.29 – 4.02 (m, 1H), 3.49 – 3.41 (m, 1H), 3.21 – 3.00 (m, 1H), 2.81 – 2.48 (m, 4H), 2.47 – 2.23 (m, 7H), 1.95 – 1.80 (m, 3H), 1.72 – 1.61 (m, 1H); ESI-MS: (*m/z*) 627.2 [M+H]⁺, 649.2 [M+Na]⁺, 625.0 [M-H]⁻; HPLC *method A*: *t_r* = 7.423 min.

Detailed procedures for the preparation of final compounds 19-22

3-(1-(7-Fluoro-9*H*-pyrimido[4,5-*b*]indol-4-yl)octahydro-6*H*-pyrrolo[2,3-*c*]pyridin-6-yl)propanenitrile (**19**)

The title compound was prepared from 3-(1-(7-fluoro-9-tosyl-9*H*-pyrimido[4,5-*b*]indol-4-yl)octahydro-6*H*-pyrrolo[2,3-*c*]pyridin-6-yl)propanenitrile (**16**) (100.0 mg, 0.19 mmol) and *Kt*BuO (151.4 mg, 1.35 mmol) were stirred in HPLC grade THF (10 mL) at rt for 1.5 h. Saturated NaCl solution (10 mL) was added and the mixture extracted with EtOAc (4 x 25 mL). Combined organic layers were dried over Na₂SO₄ and concentrated under reduced pressure. Purification of the residue by flash column chromatography (SiO₂, DCM:MeOH gradient elution from 95:5 to 91.5:8.5) gave 43 mg of a solid (61% yield); ¹H NMR (400 MHz, DMSO-*d*₆) δ 12.12 (s, 1H), 8.28 (s, 1H), 8.04 (dd, *J* = 9.0, 5.3 Hz, 1H), 7.19 (dd, *J* = 9.3, 2.6 Hz, 1H), 7.05 (td, *J* = 9.3, 2.6 Hz, 1H), 4.66 – 4.58 (m, 1H), 4.21 – 4.11 (m, 1H), 3.86 – 3.77 (m, 1H), 2.94 – 2.84 (m, 1H), 2.67 – 2.46 (m, 6H, overlap with DMSO-*d*₅ signal), 2.44 – 2.32 (m, 2H), 2.03 – 1.82 (m, 3H), 1.77 – 1.68 (m, 1H); ¹³C NMR (101 MHz, DMSO-*d*₆) δ 159.9 (d, *J* = 239.5 Hz), 157.1, 156.4, 153.3, 137.3 (d, *J* = 12.5 Hz), 123.8 (d, *J* = 9.8 Hz), 119.9, 116.3, 107.9 (d, *J* = 23.2 Hz), 97.5 (d, *J* = 25.8 Hz), 96.2, 56.5, 53.2, 52.9, 49.1, 48.5, 34.1, 26.7, 25.5, 14.8; ESI-MS: (*m/z*) 387.0 [M+Na]⁺, 363.0 [M-H]⁻; HPLC *method A*: *t_r* = 3.053 min.

3-(1-(7-Bromo-9*H*-pyrimido[4,5-*b*]indol-4-yl)octahydro-6*H*-pyrrolo[2,3-*c*]pyridin-6-yl)propanenitrile (**20**)

The title compound was prepared from 3-(1-(7-bromo-9-tosyl-9*H*-pyrimido[4,5-*b*]indol-4-yl)octahydro-6*H*-pyrrolo[2,3-*c*]pyridin-6-yl)propanenitrile (**17**) (66.0 mg, 0.11 mmol) and *K**t*BuO (89.5 mg, 0.80 mmol) were stirred in HPLC grade THF (4 mL) for 2 h. Saturated NH₄Cl solution (25 mL) was added and the mixture was extracted with EtOAc (3 x 25 mL). Combined organic layers were dried over Na₂SO₄ and concentrated under reduced pressure. Purification of the residue by flash column chromatography (SiO₂, DCM:MeOH 95.5:4.5) gave 19 mg of a beige solid (40% yield); ¹H NMR (400 MHz, DMSO-*d*₆) δ 12.13 (s, 1H), 8.30 (s, 1H), 7.99 (d, *J* = 8.8 Hz, 1H), 7.57 (d, *J* = 2.0 Hz, 1H), 7.35 (dd, *J* = 8.7, 2.0 Hz, 1H), 4.68 – 4.58 (m, 1H), 4.21 – 4.10 (m, 1H), 3.89 – 3.77 (m, 1H), 2.96 – 2.86 (m, 1H), 2.66 – 2.48 (m, 6H, overlap with DMSO-*d*₅ signal), 2.44 – 2.33 (m, 2H), 2.07 – 1.84 (m, 3H), 1.77 – 1.69 (m, 1H); ¹³C NMR (101 MHz, DMSO-*d*₆) δ 156.8, 156.6, 154.0, 137.6, 124.2, 123.0, 120.0, 118.9, 116.8, 113.6, 96.0, 56.7, 53.2, 52.9, 49.1, 48.5, 34.1, 26.7, 25.5, 14.9. ESI-MS: (*m/z*) 425.5 [M+H]⁺, 447.5 [M+Na]⁺, 423.4 [M-H]⁻; HPLC *method A*: *t*_r = 3.996 min.

3-(1-(7-Iodo-9*H*-pyrimido[4,5-*b*]indol-4-yl)octahydro-6*H*-pyrrolo[2,3-*c*]pyridin-6-yl)propanenitrile (**21**)

3-(1-(7-Iodo-9-tosyl-9*H*-pyrimido[4,5-*b*]indol-4-yl)octahydro-6*H*-pyrrolo[2,3-*c*]pyridin-6-yl)propanenitrile (**18**) (100.0 mg, 0.16 mmol) and *K**t*BuO (125.4 mg, 1.11 mmol) were stirred in HPLC grade THF (10 mL) at rt for 2 h. Saturated NaCl solution (10 mL) was added and the mixture extracted with EtOAc (4 x 20 mL). Combined organic layers were dried over Na₂SO₄ and concentrated under reduced pressure. Purification of the residue by flash column chromatography (SiO₂, DCM:MeOH gradient elution from 95:5 to 91.5:8.5) gave 47 mg of a light beige solid (62% yield); ¹H NMR (400 MHz, DMSO-*d*₆) δ 12.07 (s, 1H), 8.30 (s, 1H), 7.86 (d, *J* = 8.7 Hz, 1H), 7.74 (d, *J* = 1.4 Hz, 1H), 7.51 (dd, *J* = 8.6, 1.4 Hz, 1H), 4.66 – 4.58

(m, 1H), 4.20 – 4.10 (m, 1H), 3.87 – 3.77 (m, 1H), 2.95 – 2.86 (m, 1H), 2.68 – 2.47 (m, 6H, overlap with DMSO-*d*₅ signal), 2.43 – 2.33 (m, 2H), 2.06 – 1.83 (m, 3H), 1.78 – 1.69 (m, 1H). ESI-MS: (m/z) 473.2 [M+H]⁺, 495.1 [M+Na]⁺, 471.1 [M-H]⁻; HPLC *method A*: t_r = 4.747 min.

3-(1-(7-Ethynyl-9*H*-pyrimido[4,5-*b*]indol-4-yl)octahydro-6*H*-pyrrolo[2,3-*c*]pyridin-6-yl)propanenitrile (**22**)

A solution of 3-(1-(7-iodo-9*H*-pyrimido[4,5-*b*]indol-4-yl)octahydro-6*H*-pyrrolo[2,3-*c*]pyridin-6-yl)propanenitrile (**21**) (22.0 mg, 0.05 mmol), triethylamine (11.9 mg, 0.12 mmol) and CuI (0.89 mg, 0.005 mmol) in dry DMF (1.5 mL) was degassed and stirred in a Schlenk tube under Ar atmosphere. More triethylamine (11.9 mg, 0.12 mmol) and trimethylsilylacetylene (13.8 mg, 0.14 mmol) were added under Ar flow, followed by a small amount of bis(triphenylphosphine)palladium(II) dichloride (< 5 mg). The mixture was stirred at rt and under Ar atmosphere for 2 h, then diluted with EtOAc (40 mL) and washed with saturated NaHCO₃ solution (2 x 10 mL). The combined aqueous layers were re-extracted with EtOAc (25 mL). The combined organic layers were dried over Na₂SO₄ and concentrated under reduced pressure. Residual DMF was removed under oil pump vacuum. The brown oily residue was mixed with HPLC MeOH (5 mL) and K₂CO₃ (7.8 mg, 0.06 mmol) was added. The mixture was stirred at rt and under N₂ atmosphere for 3 h and then concentrated under reduced pressure. The residue was dissolved in EtOAc (40 mL) and the solution was washed with saturated NaHCO₃ solution (2 x 15 mL), then dried over Na₂SO₄ and concentrated under reduced pressure. Purification of the residue by flash column chromatography (SiO₂, DCM:MeOH gradient elution from 95:5 to 92.5:7.5) gave 7 mg of a beige solid (41% yield); ¹H NMR (400 MHz, DMSO-*d*₆) δ 12.10 (s, 1H), 8.30 (s, 1H), 8.06 (d, *J* = 8.5 Hz, 1H), 7.50 (d, *J* = 1.5 Hz, 1H), 7.32 (dd, *J* = 8.5, 1.5 Hz, 1H), 4.70 – 4.62 (m, 1H), 4.23 – 4.14 (m, 2H), 3.90 – 3.81 (m, 1H), 2.96 – 2.88 (m, 1H), 2.67 – 2.51 (m, 6H, overlap with DMSO-*d*₅ signal), 2.46 – 2.36 (m, 2H), 2.08 – 1.98 (m, 1H), 1.96 – 1.85 (m, 2H), 1.79 – 1.70 (m, 1H); ¹³C NMR (101 MHz, DMSO-*d*₆) δ

157.1, 156.7, 154.1, 136.2, 123.8, 122.7, 120.1, 120.4, 117.0, 114.3, 96.2, 84.2, 80.3, 56.7, 53.2, 52.9, 49.2, 48.5, 34.2, 26.7, 25.5, 14.9; ESI-MS: (m/z) 393.8 [M+Na]⁺; HPLC *method A*: t_r = 3.014 min.

Protein expression and purification

GSK-3 β was expressed using a construct (pNIC-CH vector) containing residues 26-383 followed by a C-terminal hexahistidine tag. The construct was transformed into BL21(D3)-R3-pRARE2 and the colonies were inoculated into 2X LB media containing 50 $\mu\text{g mL}^{-1}$ kanamycin and 34 $\mu\text{g/mL}$ chloramphenicol and cultured overnight at 37 °C. 10-12 mL of the overnight culture were inoculated in 1 L of TB media containing 50 $\mu\text{g/mL}$ kanamycin and cultures were grown at 37 °C with shaking until OD₆₀₀ of 1.5-1.8 was reached. After the temperature was reduced to 18 °C, IPTG was added at a final concentration of 0.5 mM to the cultures and left overnight. The cells were harvested on the next day by centrifugation at 5000 rpm for 10 minutes and the pellet was collected for the purification steps.

The pellet was resuspended in lysis buffer containing 50 mM HEPES pH 7.5, 500 mM NaCl, 30 mM imidazole, 5% glycerol and 0.5 mM TCEP. Protease inhibitor cocktail from Sigma was added to a dilution of 1:5000. The resuspended cells were lysed by sonication and cleared of DNA by addition of 0.15% polyethylenimine followed by centrifugation at 23000 rpm for 30 minutes. The supernatant was added into a gravity column containing 5 mL of 50% Ni-NTA slurry (Qiagen) previously equilibrated with 40 mL of lysis buffer. Subsequently, 100 mL of lysis buffer was used for washing the column and GSK-3 β was eluted with lysis buffer containing 50 mM, 100 mM, 200 mM and 300 mM imidazole. The eluted fractions containing the protein were pulled together and concentrated using a 10 kDa cutoff ultrafiltration unit until 5 mL and further purified by fractionation on a size exclusion chromatography (SEC) using column Hiload 16/600 Superdex 200 pre-equilibrated with SEC buffer containing 25 mM HEPES pH 7.5, 200mM NaCl, 5% glycerol and 0.5 mM TCEP. The purified protein was

concentrated to 12 mg/mL and snap frozen into liquid nitrogen. Protein identity was confirmed by electrospray ionization mass spectrometry (expected 41550.9 Da, observed 41552.0 Da).

Crystallization and structure determination

The inhibitors were added at a final concentration of 1 mM to 10 mg/mL of protein (diluted from 12 mg/mL stock using SEC buffer) incubated for minimum 1 h at 4 °C. The mixture protein:inhibitor was centrifuged to separate any insoluble material and crystals were obtained by sitting drop vapor diffusion method at 20 °C using 12% PEG 8000, 1 mM MgCl₂, 0.5M NaCl and 0.1M Tris pH 8.0 into a 300 nl drop mixing protein and precipitant at 2:1 volume ratio. The crystals were cryoprotected with a solution of precipitant and 20% ethylene glycol and flash cooled to 100 K and diffraction data were collected at Swiss Light Source station PXI-X06SA. The data were processed with XDS package⁵² and AIMLESS⁵³ and solved by molecular replacement using the program PHASER⁵⁴ implemented in the CCP4 suite⁵⁵ and the structure of GSK-3 β (PDB ID 6GN1) as searching model.⁵⁶ The asymmetric unit contained one molecule and the electron density on the ATP binding site was clearly detected. The structure was further refined upon insertion of water molecules and the ligand using REFMAC5,⁵⁷ PHENIX⁵⁸ COOT⁵⁹ and MOLPROBITY⁶⁰ was used for model validation. Data collection and refinement statistics are summarized in Table 4.

Table 4. Data collection and refinement statistics.

GSK-3 β and compound (S)- 5c (PDB 7B6F)	
Data Collection	
Resolution range (Å) ^a	42.41 - 2.05 (2.11 - 2.05)
Space group	I 1 2 1
Cell dimensions a, b, c (Å), α , β , γ (°C)	57.7, 63.1, 132.2, 90.0, 97.4, 90.0
No. unique observations ^a	28973 (2204)
Completeness (%) ^a	97.7 (96.8)
Mean $\langle(I)/\sigma(I)\rangle$ ^a	11.1 (2.2)
R _{pim} ^a	0.036 (0.373)
Mean CC (1/2) ^a	0.998 (0.713)

Multiplicity ^a	2.7 (2.5)
Refinement	
No. atoms in refinement	2928
average B factor (Å ²)	43.0
R _{work} (%)	17.4
R _{free} (%)	20.9
r.m.s deviation from ideal bond length (Å)	0.86
r.m.s deviation from ideal bond angle (°)	0.008
Molprobtity Ramachandran	
Favoured (%)	97
Outliers (%)	0

^a Values within parentheses refer to the highest-resolution shell.

Molecular Modeling

All modeling was conducted with Maestro version 2020-2 (Schrödinger LLC, New York, NY, 2020) using OPLS3e force field,⁶¹ unless otherwise stated.

For WaterMap²⁴⁻²⁵ calculations, the crystal structure was first prepared with Protein Preparation Wizard,⁶² where *e.g.* hydrogen bonds were optimized and the structure was energy minimized (RMSD restrain of 0.3 Å was applied for heavy atoms convergence). For calculations with **(S)-15** and **(S)-5m**, the co-crystallized ligand **(S)-5c** was first replaced with the aligned ligands that were prepared with LigPrep (Schrödinger LLC) and then the obtained protein–ligand structure was prepared with the Protein Preparation Wizard (as above). Water molecules within 10 Å of the retained ligand were included in the WaterMap analysis. Existing crystal structure water molecules were treated as part of the explicit solvent and simulation time of 2.0 ns was used in the WaterMap simulation, where water was described with TIP4P water model and non-solvent heavy atoms were restrained. The WaterMap analysis for the MD derived structures were run with the same settings, and the protein-ligand complexes were taken from final frames (at 1000 ns) of five MD simulation replicas, where ions and water molecules (except water within

4 Å from the ligand) were deleted before the system preparation with the Protein Preparation Wizard.

QM calculation were conducted with Jaguar.⁶³ Geometry optimization was done for the aligned ligands, which were prepared with the LigPrep, using B3LYP-D3 theory with 6-31G** basis set in gas-phase (except LACVP** for (*S*)-**11** with iodine). Atomic electrostatic potential (ESP) charges were calculated for the optimized geometries using 6-31G**++ using the PBF water as solvent model.

MD simulations we run in NPT ensemble (310 K; 1.01325 bar) using Desmond engine.⁶⁴ Simulation settings were as described earlier.⁶⁵ Protein Preparation Wizard prepared GSK-3β–(*S*)-**15** complexes were solvated in a cubic box (min. distance of 15 Å from the protein to the box edges) including K⁺ and Cl[−] ions in 0.15 M concentration with a neutral net charge for the final system. The water was described with TIP3P model.⁶⁶ Final systems consisted of 76,109 atoms. Ten replica simulations were run using a different seed for each simulation. A default Desmond relaxation protocol was applied before the 1000 ns production simulations. Water distances and locations were analysed with trajectory_asl_monitor.py script (Schrödinger LLC).

Maestro and PyMOL Molecular Graphics System (Version 2.2.3 Schrödinger, LLC) were used for visualization.

ASSOCIATED CONTENTS

Supporting Information

ADP GloTM kinase assay protocol, Figures S1-S9, NanoBRETTM target engagement assay protocol and results, materials and methods for cellular assays in neuronal SH-SY5Y cells,

kinome screening data for compounds (**S**)-**15** and **22**, ¹H and ¹³C NMR spectra as well as HPLC chromatograms of compounds (**S**)-**5c**, (**S**)-**15**, **20** and **22** (PDF).

SMILES strings of tested compounds (CSV).

Analysis of the HR-I conserved water residues in high-resolution GSK-3β crystal structures (CSV).

This material is available free of charge via the Internet at <http://pubs.acs.org>.

The raw concatenated trajectories of the MD simulations of compounds (**S**)-**5c** and (**S**)-**15** and WaterMap-output files are freely available at <https://doi.org/10.5281/zenodo.4646862>.

Acknowledgments

The authors acknowledge CSC – IT Center for Science, Finland, for computational resources. T.P. acknowledges funding from the European Union’s Horizon 2020 research and innovation programme under the Marie Skłodowska-Curie Grant agreement No 839230 and Orion Research Foundation sr. R.T. is supported by the German Research Foundation (DFG) grant 397659447. The data collection at SLS was supported by funding from the European Union’s Horizon 2020 research and innovation program grant agreement number 730872, project CALIPSOplus.

The Structural Genomics Consortium (SGC) is a registered charity (no: 1097737) that receives funds from; AbbVie, Bayer AG, Boehringer Ingelheim, Canada Foundation for Innovation, Eshelman Institute for Innovation, Genentech, Genome Canada through Ontario Genomics Institute [OGI-196], EU/EFPIA/OICR/McGill/KTH/Diamond, Innovative Medicines Initiative 2 Joint Undertaking [EUBOPEN grant 875510], Janssen, Merck KGaA (aka EMD in Canada

and US), Merck & Co (aka MSD outside Canada and US), Pfizer, São Paulo Research Foundation-FAPESP, Takeda and Wellcome [106169/ZZ14/Z].

The authors thank Jens Strobach and Maria Beer-Krön for their excellent assistance with the GSK-3 β ADP Glo and NanoBRET assay, respectively.

The data collection at Swiss Light Source (SLS) was supported by funding from the European Union's Horizon 2020 research and innovation program grant agreement number 730872, project CALIPSOplus. We thank the staff at beamline X06SA of the Swiss Light Source for assistance during data collection.

Abbreviations

BRET, bioluminescence resonance energy transfer; GSK-3 β , glycogen synthase kinase-3 β ; HPLC, high-performance liquid chromatography; HR-I, hydrophobic region I; MS, mass spectrometry; MD, molecular dynamics; S_NAr, nucleophilic aromatic substitution.

AUTHOR INFORMATION

Corresponding Author

*Corresponding author: pierre.koch@uni-tuebingen.de, pierre.koch@ur.de; Tel.: +49 941 943 4827

Notes

The authors declare no competing financial interest.

References

1. Taylor, S. S.; Meharena, H. S.; Kornev, A. P. Evolution of a dynamic molecular switch. *IUBMB Life* **2019**, *71*, 672-684.
2. Ferguson, F. M.; Gray, N. S. Kinase inhibitors: the road ahead. *Nat. Rev. Drug Discovery* **2018**, *17*, 353-377.
3. Shih, H.-P.; Zhang, X.; Aronov, A. M. Drug discovery effectiveness from the standpoint of therapeutic mechanisms and indications. *Nat. Rev. Drug Discovery* **2018**, *17*, 19-33.
4. Liu, S.-K.; Xie, H.-X.; Ge, Y.-X.; Zhnag, J.; Jiang, C.-S. An updated research of glycogen synthase kinase-3beta inhibitors: a review. *Monatsh. Chem.* **2021**, *152*, 19-33.
5. Rippin, I.; Eldar-Finkelman, H. Mechanisms and therapeutic implications of GSK-3 in treating neurodegeneration. *Cells* **2021**, *10*, 262.
6. Roca, C.; Campillo, N. E. Glycogen synthase kinase 3 (GSK-3) inhibitors: a patent update (2016-2019). *Expert Opin. Ther. Pat.* **2020**, *30*, 863-872.
7. De Simone, A.; Tumiatti, V.; Andrisano, V.; Milelli, A. Glycogen synthase kinase 3beta: a new gold rush in anti-Alzheimer's disease multitarget drug discovery? *J. Med. Chem.* **2021**, *64*, 26-41.
8. Patel, P.; Woodgett, J. R. Chapter eight - glycogen synthase kinase 3: A kinase for all pathways? *Curr. Top. Dev. Biol.* **2017**, *123*, 277-302.
9. Phukan, S.; Babu, V.; Kannoji, A.; Hariharan, R.; Balaji, V. GSK3 β : role in therapeutic landscape and development of modulators. *Br. J. Pharmacol.* **2010**, *160*, 1-19.
10. Lauretti, E.; Dincer, O.; Praticò, D. Glycogen synthase kinase-3 signaling in Alzheimer's disease. *Biochim. Biophys. Acta, Mol. Cell Res.* **2020**, *1867*, 118664.

11. Ding, L.; Billadeau, D. D. Glycogen synthase kinase-3 β : a novel therapeutic target for pancreatic cancer. *Curr. Top. Dev. Biol.* **2020**, *24*, 417-426.
12. Andreev, S.; Pantsar, T.; Ansideri, F.; Kudolo, M.; Forster, M.; Schollmeyer, D.; Laufer, S. A.; Koch, P. Design, synthesis and biological evaluation of 7-chloro-9H-pyrimido[4,5-b]indole-based glycogen synthase kinase-3 β Inhibitors. *Molecules* **2019**, *24*, 2331.
13. Ball, P. Water is an active matrix of life for cell and molecular biology. *Proc. Natl. Acad. Sci. U. S. A.* **2017**, *114*, 13327-13335.
14. Snyder, P. W.; Mecinović, J.; Moustakas, D. T.; Thomas, S. W.; Harder, M.; Mack, E. T.; Lockett, M. R.; Héroux, A.; Sherman, W.; Whitesides, G. M. Mechanism of the hydrophobic effect in the biomolecular recognition of arylsulfonamides by carbonic anhydrase. *Proc. Natl. Acad. Sci. U. S. A.* **2011**, *108*, 17889-17894.
15. Breiten, B.; Lockett, M. R.; Sherman, W.; Fujita, S.; Al-Sayah, M.; Lange, H.; Bowers, C. M.; Héroux, A.; Krilov, G.; Whitesides, G. M. Water networks contribute to enthalpy/entropy compensation in protein–ligand binding. *J. Am. Chem. Soc.* **2013**, *135*, 15579-15584.
16. Michel, J.; Tirado-Rives, J.; Jorgensen, W. L. Energetics of displacing water molecules from protein binding sites: consequences for ligand optimization. *J. Am. Chem. Soc.* **2009**, *131*, 15403-15411.
17. Spyrakis, F.; Ahmed, M. H.; Bayden, A. S.; Cozzini, P.; Mozzarelli, A.; Kellogg, G. E. The roles of water in the protein matrix: A largely untapped resource for drug discovery. *J. Med. Chem.* **2017**, *60*, 6781-6827.
18. Ladbury, J. E. Just add water! The effect of water on the specificity of protein-ligand binding sites and its potential application to drug design. *Chem. Biol. (Oxford, U. K.)* **1996**, *3*, 973-980.

19. Maurer, M.; Oostenbrink, C. Water in protein hydration and ligand recognition. *J. Mol. Recognit.* **2019**, *32*, e2810.
20. Darby, J. F.; Hopkins, A. P.; Shimizu, S.; Roberts, S. M.; Brannigan, J. A.; Turkenburg, J. P.; Thomas, G. H.; Hubbard, R. E.; Fischer, M. Water networks can determine the affinity of ligand binding to proteins. *J. Am. Chem. Soc.* **2019**, *141*, 15818-15826.
21. Krimmer, S. G.; Cramer, J.; Betz, M.; Fridh, V.; Karlsson, R.; Heine, A.; Klebe, G. Rational design of thermodynamic and kinetic binding profiles by optimizing surface water networks coating protein-bound ligands. *J. Med. Chem.* **2016**, *59*, 10530-10548.
22. Nittinger, E.; Gibbons, P.; Eigenbrot, C.; Davies, D. R.; Maurer, B.; Yu, C. L.; Kiefer, J. R.; Kuglstatter, A.; Murray, J.; Ortwine, D. F.; Tang, Y.; Tsui, V. Water molecules in protein–ligand interfaces. Evaluation of software tools and SAR comparison. *J. Comput.-Aided Mol. Des.* **2019**, *33*, 307-330.
23. Bucher, D.; Stouten, P.; Triballeau, N. Shedding light on important waters for drug design: simulations versus grid-based methods. *J. Chem. Inf. Model.* **2018**, *58*, 692-699.
24. Abel, R.; Young, T.; Farid, R.; Berne, B. J.; Friesner, R. A. Role of the active-site solvent in the thermodynamics of factor Xa ligand binding. *J. Am. Chem. Soc.* **2008**, *130*, 2817-2831.
25. Young, T.; Abel, R.; Kim, B.; Berne, B. J.; Friesner, R. A. Motifs for molecular recognition exploiting hydrophobic enclosure in protein–ligand binding. *Proc. Natl. Acad. Sci. U. S. A.* **2007**, *104*, 808-813.
26. Horbert, R.; Pinchuk, B.; Johannes, E.; Schlosser, J.; Schmidt, D.; Cappel, D.; Totzke, F.; Schächtele, C.; Peifer, C. Optimization of potent DFG-in inhibitors of platelet derived growth factor receptor β (PDGF-R β) guided by water thermodynamics. *J. Med. Chem.* **2015**, *58*, 170-182.

27. Pearlstein, R. A.; Sherman, W.; Abel, R. Contributions of water transfer energy to protein-ligand association and dissociation barriers: Watermap analysis of a series of p38 α MAP kinase inhibitors. *Proteins: Struct., Funct., Bioinf.* **2013**, *81*, 1509-1526.
28. Myrianthopoulos, V.; Kritsanida, M.; Gaboriaud-Kolar, N.; Magiatis, P.; Ferandin, Y.; Durieu, E.; Lozach, O.; Cappel, D.; Soundararajan, M.; Filippakopoulos, P.; Sherman, W.; Knapp, S.; Meijer, L.; Mikros, E.; Skaltsounis, A.-L. Novel Inverse binding mode of indirubin derivatives yields improved selectivity for DYRK kinases. *ACS Medicinal Chemistry Letters* **2013**, *4*, 22-26.
29. Robinson, D. D.; Sherman, W.; Farid, R. Understanding kinase selectivity through energetic analysis of binding site waters. *ChemMedChem* **2010**, *5*, 618-627.
30. Robinson, D.; Bertrand, T.; Carry, J.-C.; Halley, F.; Karlsson, A.; Mathieu, M.; Minoux, H.; Perrin, M.-A.; Robert, B.; Schio, L.; Sherman, W. Differential water thermodynamics determine PI3K-beta/delta selectivity for solvent-exposed ligand modifications. *J. Chem. Inf. Model.* **2016**, *56*, 886-894.
31. Asquith, C. R. M.; Tizzard, G. J.; Bennett, J. M.; Wells, C. I.; Elkins, J. M.; Willson, T. M.; Poso, A.; Laitinen, T. Targeting the water network in cyclin G-associated kinase (GAK) with 4-anilino-quin(az)oline Inhibitors. *ChemMedChem* **2020**, *15*, 1200-1215.
32. Hamaguchi, H.; Amano, Y.; Moritomo, A.; Shirakami, S.; Nakajima, Y.; Nakai, K.; Nomura, N.; Ito, M.; Higashi, Y.; Inoue, T. Discovery and structural characterization of peficitinib (ASP015K) as a novel and potent JAK inhibitor. *Bioorg. Med. Chem.* **2018**, *26*, 4971-4983.
33. Lee, K. L.; Ambler, C. M.; Anderson, D. R.; Boscoe, B. P.; Bree, A. G.; Brodfuehrer, J. I.; Chang, J. S.; Choi, C.; Chung, S.; Curran, K. J.; Day, J. E.; Dehnhardt, C. M.; Dower, K.; Drozda, S. E.; Frisbie, R. K.; Gavrin, L. K.; Goldberg, J. A.; Han, S.; Hegen, M.; Hepworth, D.; Hope, H. R.; Kamtekar, S.; Kilty, I. C.; Lee, A.; Lin, L.-L.; Lovering, F. E.; Lowe, M. D.; Mathias, J. P.; Morgan, H. M.; Murphy, E. A.; Papaioannou, N.; Patny, A.;

- Pierce, B. S.; Rao, V. R.; Saiah, E.; Samardjiev, I. J.; Samas, B. M.; Shen, M. W. H.; Shin, J. H.; Soutter, H. H.; Strohbach, J. W.; Symanowicz, P. T.; Thomason, J. R.; Trzupek, J. D.; Vargas, R.; Vincent, F.; Yan, J.; Zapf, C. W.; Wright, S. W. Discovery of clinical candidate 1- $\{[(2S,3S,4S)\text{-}3\text{-Ethyl-4-fluoro-5-oxopyrrolidin-2-yl]methoxy}\}$ -7-methoxyisoquinoline-6-carboxamide (PF-06650833), a potent, selective inhibitor of interleukin-1 receptor associated kinase 4 (IRAK4), by fragment-based drug design. *J. Med. Chem.* **2017**, *60*, 5521-5542.
34. Matricon, P.; Suresh, R. R.; Gao, Z.-G.; Panel, N.; Jacobson, K. A.; Carlsson, J. Ligand design by targeting a binding site water. *Chem. Sci.* **2021**, *12*, 960-968.
35. Andreev, S.; Pantsar, T.; El-Gokha, A.; Ansideri, F.; Kudolo, M.; Anton, D. B.; Sita, G.; Romasco, J.; Geibel, C.; Lämmerhofer, M.; Goettert, M. I.; Tarozzi, A.; Laufer, S. A.; Koch, P. Discovery and evaluation of enantiopure 9H-pyrimido[4,5-b]indoles as nanomolar GSK-3 β inhibitors with improved metabolic stability. *Int. J. Mol. Sci.* **2020**, *21*, 7823.
36. Zegzouti, H.; Zdanovskaia, M.; Hsiao, K.; Goueli, S. A. ADP-glo: A bioluminescent and homogeneous ADP monitoring assay for kinases. *Assay Drug Dev. Technol.* **2009**, *7*, 560-572.
37. Ghose, A. K.; Viswanadhan, V. N.; Wendoloski, J. J. Prediction of hydrophobic (lipophilic) properties of small organic molecules using fragmental methods: an analysis of ALOGP and CLOGP methods. *J. Phys. Chem. A* **1998**, *102*, 3762-3772.
38. Hopkins, A. L.; Keserü, G. M.; Leeson, P. D.; Rees, D. C.; Reynolds, C. H. The role of ligand efficiency metrics in drug discovery. *Nat. Rev. Drug Discovery* **2014**, *13*, 105-121.
39. Desroy, N.; Housseman, C.; Bock, X.; Joncour, A.; Bienvenu, N.; Cherel, L.; Labeguerre, V.; Rondet, E.; Peixoto, C.; Grassot, J.-M.; Picolet, O.; Annoot, D.; Triballeau, N.; Monjardet, A.; Wakselman, E.; Roncoroni, V.; Le Tallec, S.; Blanque, R.; Cottreaux, C.; Vandervoort, N.; Christophe, T.; Mollat, P.; Lamers, M.; Auberval, M.; Hrvacic, B.; Ralic, J.; Oste, L.; van der Aar, E.; Brys, R.; Heckmann, B. Discovery of 2- $[[2\text{-ethyl-6-[4-[2-(3-hydroxyazetidin-1-yl)-2-oxoethyl]piperazin-1-yl]-8-methylimidazo[1,2-a]pyridin-3-$

yl]methylamino]-4-(4-fluorophenyl)thiazole-5-carbonitrile (GLPG1690), a first-in-class autotaxin inhibitor undergoing clinical evaluation for the treatment of idiopathic pulmonary fibrosis. *J. Med. Chem.* **2017**, *60*, 3580-3590.

40. Kung, P.-P.; Sinnema, P.-J.; Richardson, P.; Hickey, M. J.; Gajiwala, K. S.; Wang, F.; Huang, B.; McClellan, G.; Wang, J.; Maegley, K.; Bergqvist, S.; Mehta, P. P.; Kania, R. Design strategies to target crystallographic waters applied to the Hsp90 molecular chaperone. *Bioorg. Med. Chem. Lett.* **2011**, *21*, 3557-3562.

41. Henzler-Wildman, K.; Kern, D. Dynamic personalities of proteins. *Nature* **2007**, *450*, 964-972.

42. Pruccoli, L.; Morroni, F.; Sita, G.; Hrelia, P.; Tarozzi, A. Esculetin as a bifunctional antioxidant prevents and counteracts the oxidative stress and neuronal death induced by amyloid protein in SH-SY5Y cells. *Antioxidants* **2020**, *9*, 551.

43. Lochhead, P. A.; Kinstrie, R.; Sibbet, G.; Rawjee, T.; Morrice, N.; Cleghon, V. A chaperone-dependent GSK3 β transitional intermediate mediates activation-loop autophosphorylation. *Mol. Cell* **2006**, *24*, 627-633.

44. Cole, A.; Frame, S.; Cohen, P. Further evidence that the tyrosine phosphorylation of glycogen synthase kinase-3 (GSK3) in mammalian cells is an autophosphorylation event. *Biochem. J.* **2004**, *377*, 249-255.

45. Wagner, F. F.; Benajiba, L.; Campbell, A. J.; Weïwer, M.; Sacher, J. R.; Gale, J. P.; Ross, L.; Puissant, A.; Alexe, G.; Conway, A.; Back, M.; Pikman, Y.; Galinsky, I.; DeAngelo, D. J.; Stone, R. M.; Kaya, T.; Shi, X.; Robers, M. B.; Machleidt, T.; Wilkinson, J.; Hermine, O.; Kung, A.; Stein, A. J.; Lakshminarasimhan, D.; Hemann, M. T.; Scolnick, E.; Zhang, Y.-L.; Pan, J. Q.; Stegmaier, K.; Holson, E. B. Exploiting an Asp-Glu “switch” in glycogen synthase kinase 3 to design paralog-selective inhibitors for use in acute myeloid leukemia. *Sci. Transl. Med.* **2018**, *10*, eaam8460.

46. Tarozzi, A.; Morroni, F.; Merlicco, A.; Hrelia, S.; Angeloni, C.; Cantelli-Forti, G.; Hrelia, P. Sulforaphane as an inducer of glutathione prevents oxidative stress-induced cell death in a dopaminergic-like neuroblastoma cell line. *J. Neurochem.* **2009**, *111*, 1161-1171.
47. Eid, S.; Turk, S.; Volkamer, A.; Rippmann, F.; Fulle, S. KinMap: a web-based tool for interactive navigation through human kinome data. *BMC Bioinf.* **2017**, *18*, 16.
48. Young, J. R.; Lim, J.; Machacek, M. R.; Taoka, B. M.; Otte, R. D. Inhibitors of janus kinases. WO2009075830, 2009.
49. Senecal, T. D.; Shu, W.; Buchwald, S. L. A general, practical palladium-catalyzed cyanation of (hetero)aryl chlorides and bromides. *Angew. Chem. Ind. Ed.* **2013**, *52*, 10035-10039.
50. Levinson, N. M.; Boxer, S. G. A conserved water-mediated hydrogen bond network defines bosutinib's kinase selectivity. *Nat. Chem. Biol.* **2014**, *10*, 127-32.
51. Heider, F.; Pantsar, T.; Kudolo, M.; Ansideri, F.; De Simone, A.; Pruccoli, L.; Schneider, T.; Goettert, M. I.; Tarozzi, A.; Andrisano, V.; Laufer, S. A.; Koch, P. Pyridinylimidazoles as GSK3 β inhibitors: the impact of tautomerism on compound activity via water networks. *ACS Medicinal Chemistry Letters* **2019**, *10*, 1407-1414.
52. Kabsch, W. XDS. *Acta Crystallogr., Sect. D: Biol. Crystallogr.* **2010**, *66*, 125-132.
53. Evans, P. An introduction to data reduction: space-group determination, scaling and intensity statistics. *Acta Crystallogr., Sect. D: Biol. Crystallogr.* **2011**, *67*, 282-292.
54. McCoy, A. J.; Grosse-Kunstleve, R. W.; Adams, P. D.; Winn, M. D.; Storoni, L. C.; Read, R. J. Phaser crystallographic software. *J. Appl. Crystallogr.* **2007**, *40*, 658-674.
55. Winn, M. D.; Ballard, C. C.; Cowtan, K. D.; Dodson, E. J.; Emsley, P.; Evans, P. R.; Keegan, R. M.; Krissinel, E. B.; Leslie, A. G. W.; McCoy, A.; McNicholas, S. J.; Murshudov, G. N.; Pannu, N. S.; Potterton, E. A.; Powell, H. R.; Read, R. J.; Vagin, A.; Wilson, K. S. Overview of the CCP4 suite and current developments. *Acta Crystallographica Section D* **2011**, *67*, 235-242.

56. Tesch, R.; Becker, C.; Müller, M. P.; Beck, M. E.; Quambusch, L.; Getlik, M.; Lategahn, J.; Uhlenbrock, N.; Costa, F. N.; Polêto, M. D.; Pinheiro, P. d. S. M.; Rodrigues, D. A.; Sant'Anna, C. M. R.; Ferreira, F. F.; Verli, H.; Fraga, C. A. M.; Rauh, D. An unusual intramolecular halogen bond guides conformational selection. *Angew. Chem. Int. Ed.* **2018**, *57*, 9970-9975.
57. Murshudov, G. N.; Skubak, P.; Lebedev, A. A.; Pannu, N. S.; Steiner, R. A.; Nicholls, R. A.; Winn, M. D.; Long, F.; Vagin, A. A. REFMAC5 for the refinement of macromolecular crystal structures. *Acta Crystallogr., Sect. D: Biol. Crystallogr.* **2011**, *67*, 355-367.
58. Liebschner, D.; Afonine, P. V.; Baker, M. L.; Bunkoczi, G.; Chen, V. B.; Croll, T. I.; Hintze, B.; Hung, L. W.; Jain, S.; McCoy, A. J.; Moriarty, N. W.; Oeffner, R. D.; Poon, B. K.; Prisant, M. G.; Read, R. J.; Richardson, J. S.; Richardson, D. C.; Sammito, M. D.; Sobolev, O. V.; Stockwell, D. H.; Terwilliger, T. C.; Urzhumtsev, A. G.; Videau, L. L.; Williams, C. J.; Adams, P. D. Macromolecular structure determination using X-rays, neutrons and electrons: recent developments in Phenix. *Acta Crystallogr., Sect. D: Biol. Crystallogr.* **2019**, *75*, 861-877.
59. Emsley, P.; Lohkamp, B.; Scott, W. G.; Cowtan, K. Features and development of Coot. *Acta Crystallogr., Sect. D: Biol. Crystallogr.* **2010**, *66*, 486-501.
60. Chen, V. B.; Arendall, W. B., III; Headd, J. J.; Keedy, D. A.; Immormino, R. M.; Kapral, G. J.; Murray, L. W.; Richardson, J. S.; Richardson, D. C. MolProbity: all-atom structure validation for macromolecular crystallography. *Acta Crystallogr., Sect. D: Biol. Crystallogr.* **2010**, *66*, 12-21.
61. Roos, K.; Wu, C.; Damm, W.; Reboul, M.; Stevenson, J. M.; Lu, C.; Dahlgren, M. K.; Mondal, S.; Chen, W.; Wang, L.; Abel, R.; Friesner, R. A.; Harder, E. D. OPLS3e: Extending force field coverage for drug-like small molecules. *J. Chem. Theory Comput.* **2019**, *15*, 1863-1874.

62. Madhavi Sastry, G.; Adzhigirey, M.; Day, T.; Annabhimoju, R.; Sherman, W. Protein and ligand preparation: parameters, protocols, and influence on virtual screening enrichments. *J. Comput.-Aided Mol. Des.* **2013**, *27*, 221-234.
63. Bochevarov, A. D.; Watson, M. A.; Greenwood, J. R.; Philipp, D. M. Multiconformation, density functional theory-based pKa prediction in application to large, flexible organic molecules with diverse functional groups. *J. Chem. Theory Comput.* **2016**, *12*, 6001-6019.
64. Bowers, K. J.; Chow, E.; Xu, H.; Dror, R. O.; Eastwood, M. P.; Gregersen, B. A.; Klepeis, J. L.; Kolossvary, I.; Moraes, M. A.; Sacerdoti, F. D.; Salmon, J. K.; Shan, Y.; Shaw, D. E., Scalable algorithms for molecular dynamics simulations on commodity clusters. In *Proceedings of the 2006 ACM/IEEE conference on Supercomputing*, ACM: Tampa, Florida, 2006; p 84.
65. Pantsar, T. KRAS(G12C)–AMG 510 interaction dynamics revealed by all-atom molecular dynamics simulations. *Sci. Rep.* **2020**, *10*, 11992.
66. Jorgensen, W. L.; Chandrasekhar, J.; Madura, J. D.; Impey, R. W.; Klein, M. L. Comparison of simple potential functions for simulating liquid water. *J. Chem. Phys.* **1983**, *79*, 926-935.

Table of Contents graphic

